TALLINNA TEHNIKAÜLIKOOL
TALLINN UNIVERSITY OF TECHNOLOGY

Department of Electrical Power Engineering and Mechatronics

SIMULATION OF HUMAN WALKING ON THE "TOE-TO-GROUND" PHASE

ASTUMISE FAASI SIMULEERIMINE INIMESE KÄIMISEL

MASTER THESIS

Student: Assel Nurmukhanova.....
/name/

Student code 174823MAHM.....

Supervisor: Prof. Mart Tamre.....
/name, position/

Tallinn, 2019

AUTHOR'S DECLARATION

Hereby I declare, that I have written this thesis independently.
No academic degree has been applied for based on this material. All works, major viewpoints and data of the other authors used in this thesis have been referenced.

"....." ..... 201…..

Author: Assel Nurmukhanova
/signature /

Thesis is in accordance with terms and requirements

"....." ..... 201….

Supervisor: Prof. Mart Tamre
/signature/

Accepted for defence

"....."..... 201… .

Chairman of theses defence commission: .....
/name and signature/

Department of Electrical Power Engineering and Mechatronics

THESIS TASK

Student: Assel Nurmukhanova, 174823MAHM

Study programme, MAHM Mechatronics

main speciality:

Supervisor(s): Prof. Mart Tamre, +372 6203202

Consultants Prof, Musalimov Viktor Mikhailovich (ITMO), musvm@yandex.ru

Thesis topic:

(in English) Simulation of human walking on the "toe-to-ground" phase

(in Estonian) Astumise faasi simuleerimine inimese käimisel

Thesis main objectives:

1. Analysis of the initial experimental data
2. Selection of the theoretical applications for describing a human walking on the basis of the experimental data
3. Modeling of the movement of the human MSS in the contact phase for a flat case, as well as modeling MSS movement taking into account the tibial rotation

Thesis tasks and time schedule:

No	Task description	Deadline
1.	Acquaintance with experimental data and their processing	15.10.2018
2.	Musculoskeletal system movement simulation in the phase of contact (plant case)	25.10.2018
3.	Movements simulation with regard to the rotation of the leg	07.11.2018
4.	Model calculation and analysis of these calculations	25.11.2018

Language: english **Deadline for submission of thesis:** " 03 " january 2019

Student: Assel Nurmukhanova ..... "....."....201….a

/signature/

Supervisor: …… ..... "....."....201….a

/signature/

Consultant: …… ..... "....."....201….a

/signature/

Table of contents

List of abbreviations and symbols

°	degree
COM	Center of mass
COP	Center of pressure
et al.	et alia
i.e.	that is
LT	Left
MSS	Musculoskeletal system
RT	Right

1. INTRODUCTION

Biomechatronics is an applied interdisciplinary science, which object of study is the interaction of biological and mechatronic systems in all its aspects. It merges the best developments in mechanics, control theory and data processing, machine vision, electronics, biology and medicine. With the term biomechatronic systems are often considered intelligent prostheses and orthosis, however this area is much wider. In addition to the arms and legs, there are many human organs, functions of which can be enhanced by introducing “Smart Systems”.

The basic knowledge in biomechatronics is understanding how the complex system of the human body works: how it moves, exchanges information and energy. Motion capture systems such as optical systems (markers and high-speed cameras) and kinesthetic, consisting of mechanical displacement and inertial sensors can answer the questions on how all the components of the musculoskeletal human apparatus coordinate during walking, running and other exercises [14].

Creating mathematical models of the musculoskeletal system (MSS) remains an actual problem. It has happened due to such circumstances, as updating experimental data and the development of a theoretical basis for the synthesis of biomechatronic and robotic systems.

Nowadays, scientists and researchers try to better understand the relationship between the human motor control systems and walking dynamics. The athletes and their coaches use human walking analyzing methods in regards to running, in order to enhance the performance without any injuries. Companies, specialized on manufacturing sport equipment seek to estimate the expected benefit of their products in comparison with the competitors. Human walking analysis is a base for medical specialists in the creation efficient rehabilitation protocols.

The purpose of this work is an experimental-mathematical modeling of human walking based on experimental data, obtained using optical markers and the platform that measures pressure and ground reaction force.

During the work, the following tasks were performed:

1. Analysis of the initial experimental data;
2. Analysis of the studies conducted by other researchers;
3. Selection of the theoretical applications for describing a human walking on the basis of the experimental data;
4. Modeling of the movement of the human MSS in the contact phase for a flat case, as well as modeling MSS movement taking into account the tibial rotation;

Chapter 2 describes the basic methods for obtaining experimental data on human walking.

Chapter 3 describes the theoretical means by which we simulate human walking.

Chapter 4 is devoted to the analysis of the results of experiments conducted in the laboratory of the University of Tartu.

2. WALKING RESEARCH METHODS OVERVIEW

For human walking analysis, data can be collected by different methods. Motion sensors and systems, such as the gyroscope, the accelerometer, strain gauges, force sensors, goniometers and electromyography sensors can measure various characteristics of human walking. Experiments can be performed either based on a single type sensors or on a combined sensor system of multiple types of sensors [31,32].

Another one approach of research method is based on using pins inserted into the bones.

A standard human walking analysis method is based on the motion capture system and force platform, which can measure ground-reaction forces [29, 30].

The features and basic principles of several experiments are described in the following.

2.1 Experiments with an optical marker method of motion capture

Japanese researchers investigated different walking styles, including the traditional Nanba-style walking, which could reduce the traction coefficients. Common characteristics of the Nanba-style walking, different from modern normal-style walking are as follows. In the normal-style walking, the body trunk is twisted because the right (left) arm is swung forward, while the left (right) leg steps forward. On the other hand in the Nanba-style walking, a right (left) shoulder moves forward, as a right (left) leg steps forward [28].

Figure 2.1.1 shows a schematic diagram of modern style walking and Nanba-style walking.

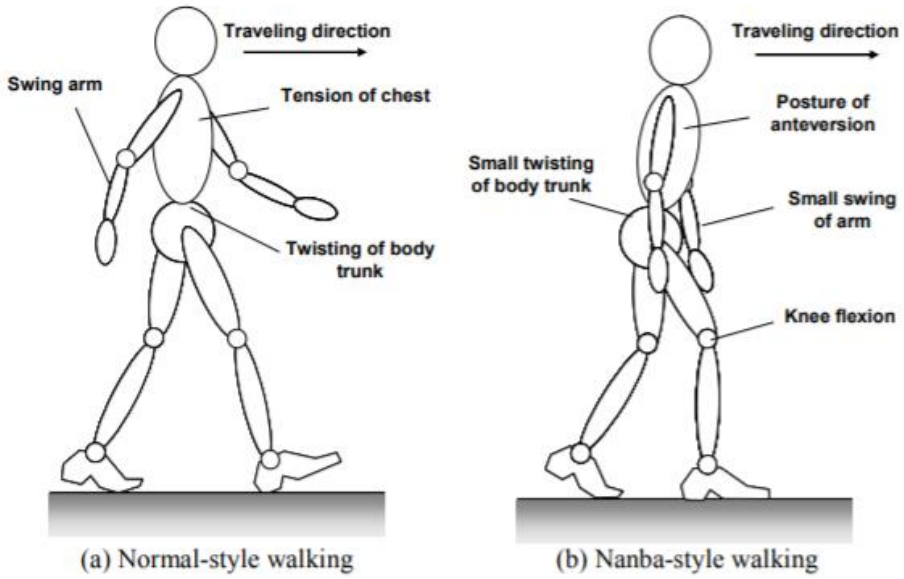

Figure 2.1.1 Schematic diagram of modern style walking and Nanba-style walking [28]

Four healthy male adults between the ages of 22 and 45 years participated in the experiment. Three orthogonal components of ground reaction force were collected with force plate arrays to calculate the traction coefficient between a shoe sole and a floor. Full body kinematics was recorded using three dimensional motion capture system (vicon 612, Vicon Motion Systems Ltd.). Each subject was tested under a wide range of step lengths and walking speeds in a normal-style or in a Nanba-style walking [28].

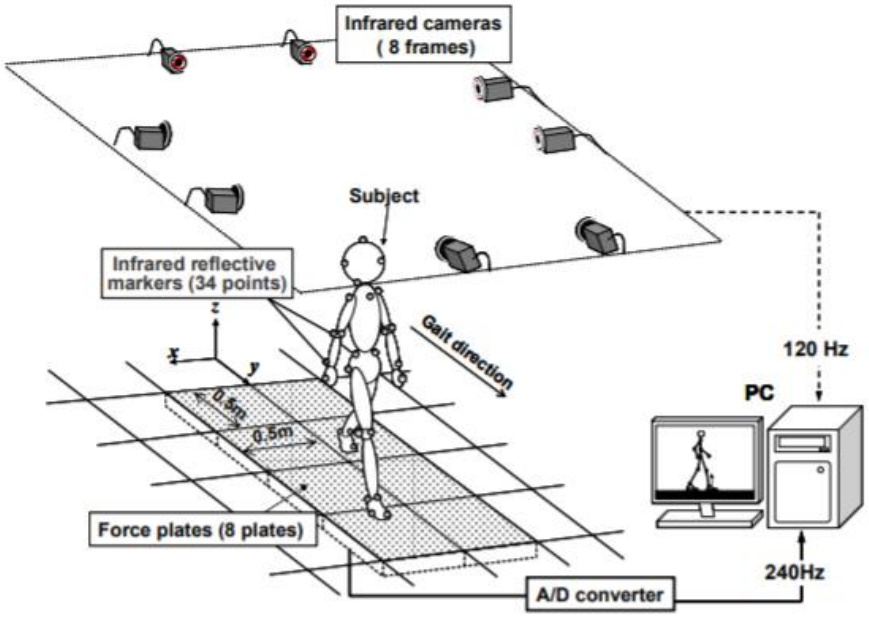

Figure 2.1.1 Schematic diagram of experimental setup for gait experiments [28]

Japanese studies were interested on the reducing of the traction coefficient between the shoe sole and the floor. They found significant differences in the ground reaction force between the normal-style walking and the Nanba-style walking. (Figure 2.1.2)

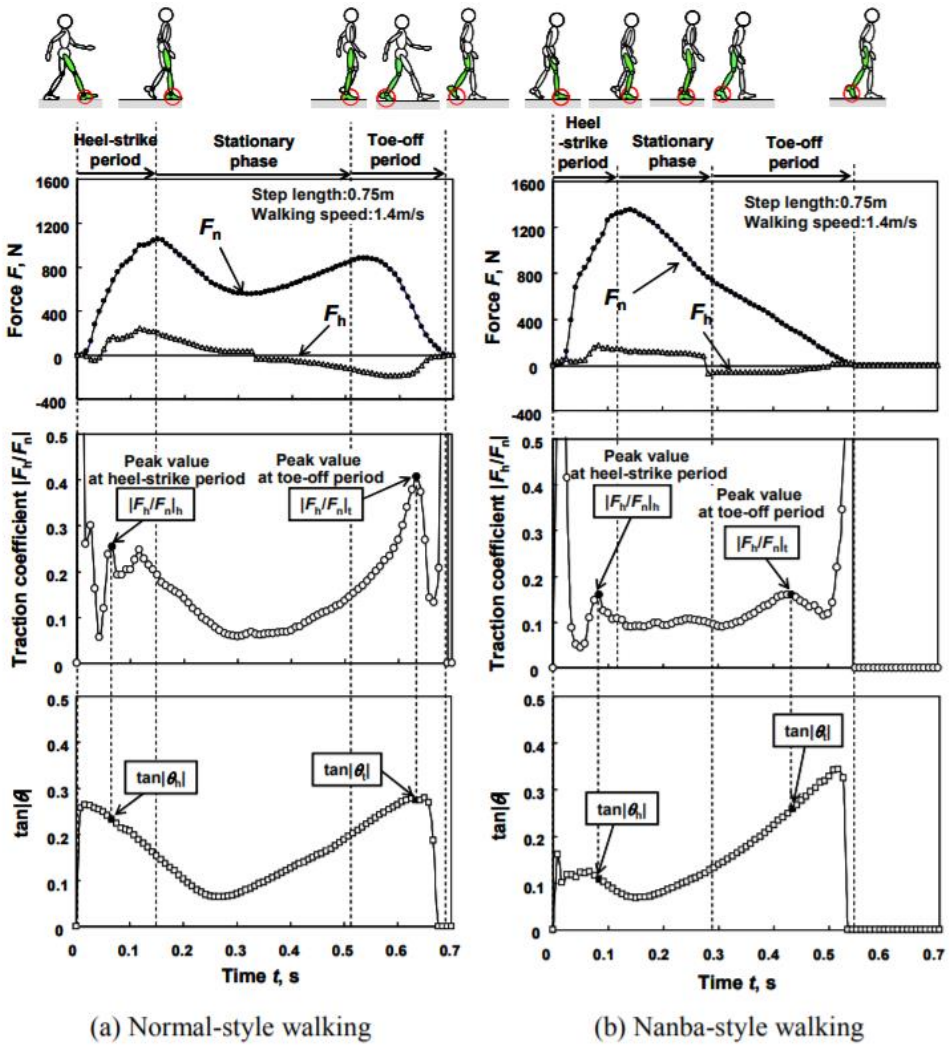

Figure 2.1.2 Ground reaction forces, traction coefficients, and $\tan|\theta|$ of each walking style [28]

After the experiments it was found that the maximum peak value of traction coefficient at heel-strike period of the Nanba style walking was significantly smaller than that of the normal style walking. The kinematic analysis investigating the geometric relationship between the whole body COM and the foot COP indicated that walking with the flexion of knees and the anteversion of the upper body found in the Nanba style walking placed the whole body COM position anterior which resulted in decrease of the distance between the COM and the COP in horizontal-plane. Such type of walking can be effective to reduce the peak traction coefficients, the slip potential, during walking.

2.2 Experiments with the additional use of accelerometers

A motion analyzer based on a three-axis accelerometer, gyroscope, magnetometer and GPS receiver G-WALK from BTS, is used for the investigation of preoperative, postoperative and rehabilitation periods, for detecting human motor disorders.

Wireless electromyography BTS FREEEMG 100RT system is used to study the muscle activity. In order to obtain an additional data channel for knee joint angles, electromyographs are used together with the sensors, measuring angles between planes - goniometers (wired and wireless) [6].

Accelerometer measures acceleration along its sensitive sensors. This type of these sensors are used for solving problems of fixing human limb movement parameters. These devices are inexpensive and compact, due to which it is possible to provide high quality assistance to more patients.

Researchers obtained kinematic and dynamic parameters describing human motion by an optical system consisting of ten Bonita cameras [20]. Locations of the markers for the optical system are shown in Figure 2.2.1 (a) (point 4 is on the back of the leg). The inertial system consists of three accelerometers gy-61 and the board Arduino Mega. The location of the sensors on the leg is shown in Figure 2.2.1 (b).

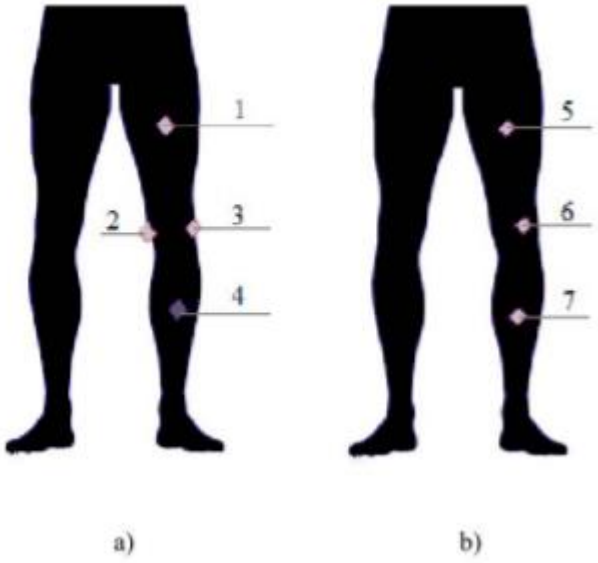

Figure 2.2.1 Location of the markers and accelerometers [20]

a) location of the optical system's markers,

b) location of the accelerometers.

2.3 Experiments with the use of Steinmann traction pins

The knee is one of the most complex synovial joints in the human body. Due its importance in daily activities and due to high rate of joint injuries, which could lead to human disability, it has been well studied by researchers. The knee joint has two functions:

1. allow movement during locomotion;
2. ensure static stability.

Knee provides necessary mobility, required for the human movement and helps to orient and position the foot in order to overcome a possible ground [5,24].

Experimental studies of the knee joint kinematics.

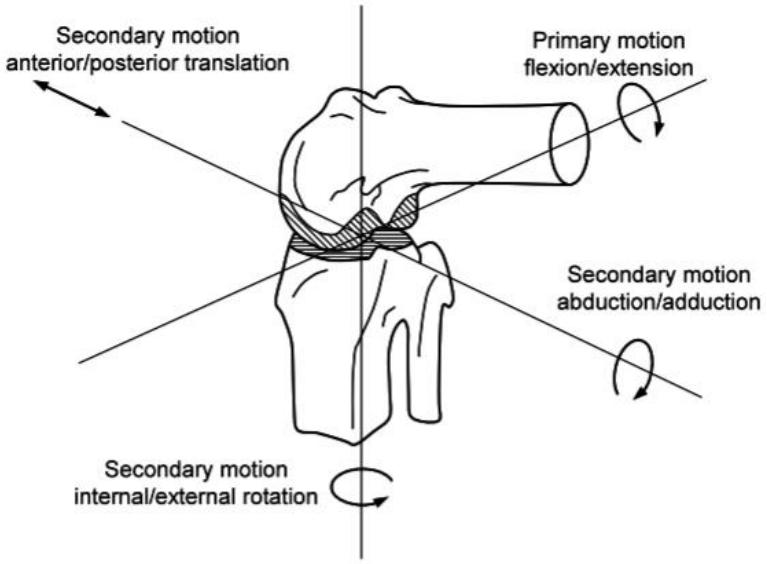

Figure 2.3.1 Femoral and tibia bone displacement during the human walking [24]

The researchers have found that the hip and tibia bones make angular displacements relative to each other along anatomical axes. (Figure 2.3.1).

- primary flexion-extension motion;
- secondary internal-external tibia rotation motion;
- secondary abduction-adduction motion.

However, the marker configurations and primarily the error due to skin movement artifacts limit the accuracy of the motion recovery [24]. This limitation particularly has effect on the measurement of more subtle secondary movements. Reliable observations of detailed knee kinematics are therefore difficult to obtain, Portuguese studies based on the experimental data from in vivo bone studies performed by Lafortune et al. [17].

Five healthy male adults (a mean age of 27.2 years, mean height 180.6 cm and a mean weight of 75.2 kg) with healthy knee joints participated in this study. Steinmann traction pins (3.2 mm diameter) were inserted with a manual orthopedic drill into the cortices of the right femur and tibia of the five subjects. Once the pins were inserted and the targets attached, radiographs of the lower limb were taken from

four different views. Thus there was obtained 3-D reconstruction of the kinematics free from the influence of soft tissue artifac [17].The pin penetrated the bone in a postero-medial direction from the anterior lateral border as shown in Figure 2.3.2 (a) and (b).

Figure 2.3.2 Radiographic view of the femoral and tibia anatomical frames of reference [17]

a) Sagittal radiographic view of the femoral and tibia anatomical frames of reference. Positive 2 axes are directed proximally and positive Y axes are directed anteriorly.

b) Frontal radiographic view of the femoral and tibia anatomical frames of reference. Positive X axes are directed laterally.

Necessary elements of walking movements are flexion and extension, while secondary movements take on the applied load carrying out energy recovery.

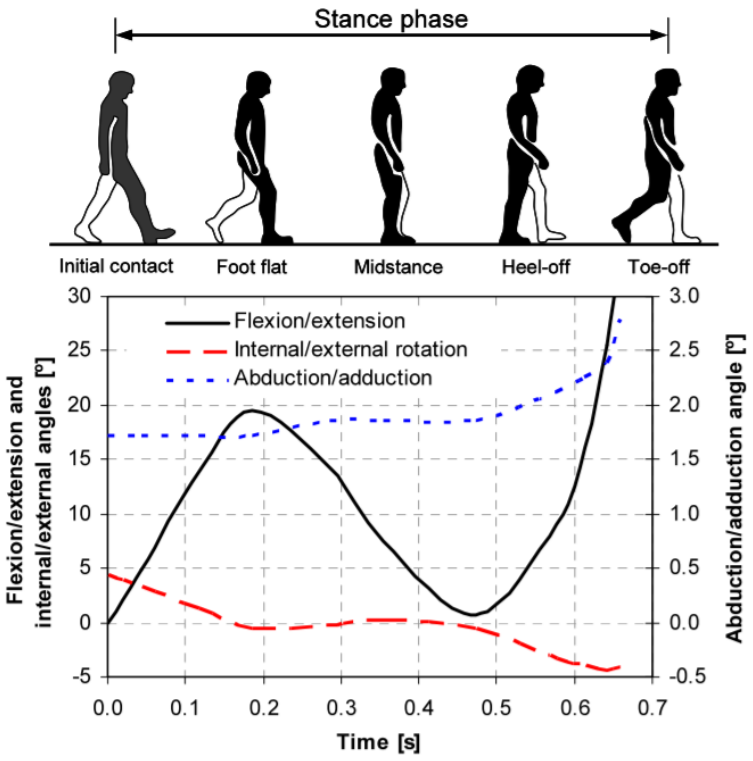

Figure 2.3.3 Angular motions of the tibia-femoral joint for the stance phase [24]

The stance phase comprises about 60% of the walking cycle for each leg and is responsible for the generation of most amount if knee force. The stance phase begins with heel strike and is followed by a double support phase in which both feet touch the ground. From toe-off of the opposite leg follows the single support phase. The swing phase begins with toe off [9, 10].

During stance phase, the ground reaction forces cause compression in the knee, which is carried by contact forces between the femoral condyles and the tibial plateau. These bony surfaces are incongruent, but the soft tissues forming the menisci and articular cartilage offer some amount of congruency against the two bony surfaces.

Figure 2.3.3 shows the angular motions of the tibia-femoral movement during the stance phase, i.e., the flexion/extension motion, the abduction/adduction motion and internal/external rotation. The graphs displays the average of the five tests obtained by Lafortune et al. [17]. The patterns start at heel

strike and end with toe-off. The flexion/extension motion comprises two flexion events and one extension event during the stance phase. Starting from the first contact, when the knee is almost fully extended, the knee flexes approximately 13.8°. At opposite toe off, the first period of single support, the knee is continuing to flex to reach the peak of stance phase flexion at about 19.5°. After this period of knee flexion, the knee starts to extend again, reaching a maximum of 0.6° close to instant of heel rise. From heel rise to toe-off, the knee flexes about 30.0°. Unlike the complex flexion/extension pattern, abduction/adduction of the tibia-femoral joint is practically uniphasic and is limited to about 1.8°. From heel strike and shortly before toe-off (approximately 0.6 seconds), there were no abduction/adduction motion and the tibia-femoral joint remains abducted approximately 0.6 degrees. Finally, the internal/external rotation occurs in a pattern somewhat similar to the flexion/extension, although with total angle variation less than 10° over the stance phase.

A better understanding of the correlation between flexion/extension and tibial internal/external rotation can be obtained by plotting one as a function of the other. Figure 2.3.4 displays the tibial rotation as a function of the flexion angle for five subjects of the study by Lafortune et al. [17].

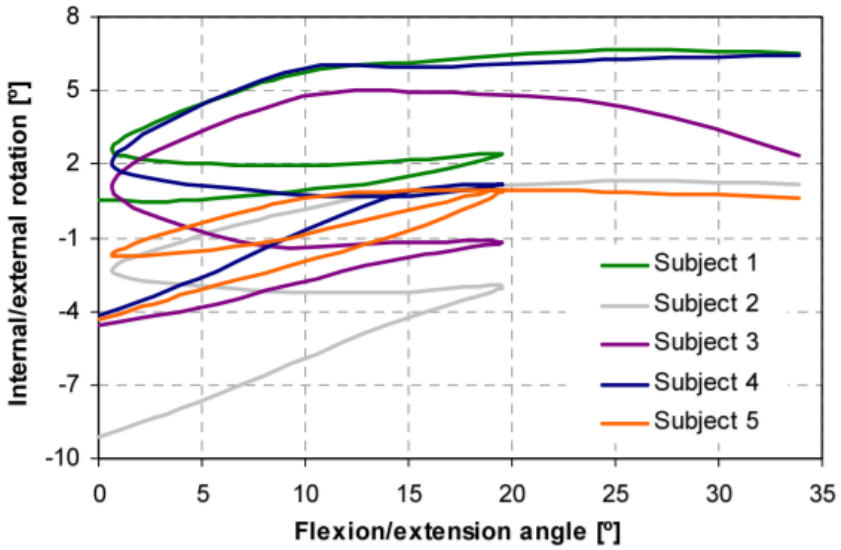

Figure 2.3.4 Angular pattern of the internal/external rotation versus knee flexion/extension angle during stance phase for the five subjects [24]

	Maximum range of the internal/external rotation [°]
Subject 1	6.1
Subject 2	10.3
Subject 3	6.9
Subject 4	10.6
Subject 5	4.9

Figure 2.3.5 Inter-individual differences in the internal/external rotation [24]

The main results obtained during experiment of Ana Ribeiro et al. with the proposed knee model have very similar tendencies as the recorded data. Figure 2.3.6 shows, that the multibody model despite to the empirical observations gives a exceptional connection between flexion/extension and tibial rotation, but it closely presents the average tendency. A possible explanation is that the observed non-unique behavior is the result of deformation of the soft tissues in the knee joint, which leads to a deviation of the kinematics of a solid body, which depends on the forces acting over the knee. This observation enables a new way to understand how the knee joint with one degree-of freedom with a complex kinematic behavior specify the shapes of the contacting surfaces, reinforced by elastic deformations.

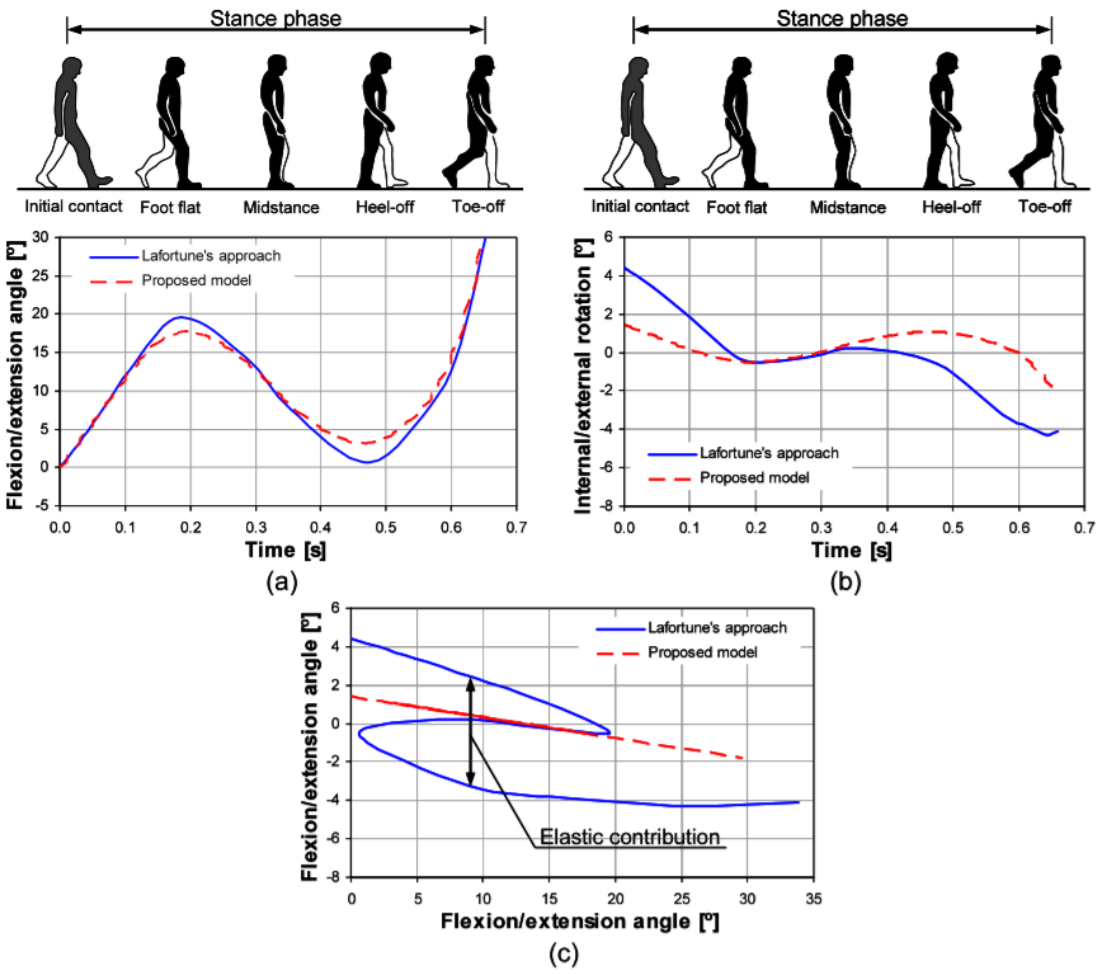

Figure 2.3.6 (a) Flexion/extension knee angle; (b) Internal/external knee rotation; (c) Angular pattern of the internal/external rotation versus knee flexion/extension angle during stance phase [24]

2.4 Conclusion

During the overview of the methods of data collection of human walking the most popular are accelerometer and motion capture system along with the platform, which measures applied force and pressure. Another approach with insertion of Steinmann traction pins is a highly invasive and stressful to measure the motion. However, this technique is very effective for studying small angles of tibia femoral rotation as are the translatory motions of the tibia when the shift is less than 6 mm.

Analyzing the results obtained by Japanese researchers, it was revealed that Nanba-style walking allows reduce the friction coefficient as well as the slip potential during human walking.

The research results of Ana Ribeiro et al. showed that the knee joint can be considered as a complex kinematic system with one degree of freedom, with a complex kinematic behavior.

For the subsequent analytical and mathematical modeling of human motion, it is necessary to find a simple law that would describe the kinematics of motion. And also that would take into account the effect of the redistribution of energy during walking.

3. ANALYTICAL INTRODUCTION

3.1 Catastrophe theory

For the analysis of the results of knee joint kinematics, catastrophe theory turned out to be the most productive.

Catastrophe theory is a method for describing the evolution of forms in nature. It was invented by Ren´e Thom in the 1960's. Thom expounded the philosophy behind the theory in his 1972 book Structural stability and morphogenesis. Catastrophe theory is particularly applicable where gradually changing forces produce sudden effects.

The applications of catastrophe theory in classical physics (or more generally in any subject governed by a 'minimization principle') help us understand what diverse models have in common. The theory has also been applied in the social and biological sciences [3].

3.1.1 Fold catastrophe

Projecting a sphere on a plane creates a fold [3].

$$A_2 : F(x;a) = \frac{1}{3}x^3 + ax \qquad (3.1.1.1)$$

The number of critical points depends from a:

$a < 0$ - 2 critical points

$a = 0$ - 1 twice-degenerate critical point

$a > 0$ - not a single critical point

$$\nabla F = x^2 + a = 0 \tag{3.1.1.2}$$

Critical points are equal to:

$$\left.\begin{array}{l} x = -\sqrt{-a} \\ x = +\sqrt{-a} \end{array}\right| \Rightarrow F = \frac{1}{3}\left[-\sqrt{-a}\right]^3 + a\left[-\sqrt{-a}\right] = \frac{1}{3}\left[-a^{3/2}\right] + \left[-a^{3/2}\right] = |a|^{3/2}\left[\frac{1}{3}+1\right] = \frac{4}{3}|a|^{3/2} \tag{3.1.1.3}$$

$$\frac{\partial^2 F}{\partial x^2} = 2x = 2 \cdot \mp\sqrt{-a} = \mp 2|a|^{1/2} \tag{3.1.1.4}$$

3.1.2 Cusp catastrophe

Projecting the surface, that is given by the formulas 3.1.2.1 on a plane creates a cusp [3].

$$\begin{array}{l} y_1 = x_1^3 + x_1 x_2, \\ y_2 = x_2 \end{array} \tag{3.1.2.1}$$

$$A_3 : F(x;a,b) = \frac{1}{4}x^4 + \frac{1}{2}ax^2 + bx,\ (a,b) \in R^2 \tag{3.1.2.2}$$

$\nabla F = x^3 + ax + b = 0$ - executable at critical points (3.1.2.3)

$\frac{\partial^2 F}{\partial x^2} = 3x^2 + a = 0$ - executable at twice degenerate critical points (3.1.2.4)

$\frac{\partial^3 F}{\partial x^3} = 6x = 0$ - executable at three times degenerate critical points (3.1.2.5)

Position of the point parameters $a,b \in R^2$ in the space that describes a function from three times degenerate point is defined as follows:

$$\begin{array}{c} \overset{(3.1.2.5)}{\Rightarrow}\ x=0 \overset{(3.1.2.4)}{\Rightarrow}\ a=0 \overset{(3.1.2.3)}{\Rightarrow}\ b=0 \\ \Downarrow \\ F\left(x;a,b\right)=F\left(x;0,0\right)=\frac{x^4}{4} \end{array} \qquad (3.1.2.6)$$

If $x=0$, function F have three times degenerate point.

Twice degenerate point is defined as follows:

$$\begin{array}{c} \overset{(3.1.2.4)}{\Rightarrow}\ a=-3x^2 \overset{(3.1.2.3)}{\Rightarrow}\ \underbrace{x^3-3x^2x+b=0}_{\Downarrow} \\ b=2x^3 \end{array} \qquad (3.1.2.7)$$

Denote the position of the twice degenerate critical point by X_c, the formula above gives us the values of the control parameters a,b, describing the function with twice degenerate point.

Rewrite:

$$\begin{array}{c} a=-3x^2; \qquad b=2x^3 \\ x=\left(-\frac{a}{3}\right)^{1/2} \qquad x=\sqrt[3]{\frac{b}{2}} \\ \left(-\frac{a}{3}\right)^{1/2}=\left(\frac{b}{2}\right)^{1/3} \\ \Downarrow \\ \left[\left(-\frac{a}{3}\right)^{1/2}\right]^6=\left[\left(\frac{b}{2}\right)^{1/3}\right]^6 \\ \left(-\frac{a}{3}\right)^3=\left(\frac{b}{2}\right)^2 \\ \left(\frac{a}{3}\right)^3+\left(\frac{b}{2}\right)^2=0 \ \text{fold line} \end{array} \qquad (3.1.2.8)$$

Position of critical points in the space is found by solving the cubic equation:

$$\nabla F = x^3 + ax + b = 0 \tag{3.1.2.9}$$

Formula 3.1.2.9 defines a two dimensional manifold located in three dimensional space with coordinate axes $x - a - b$

Critical values are evaluated by subsequent substitution of the values of critical points in 3.1.2.2.

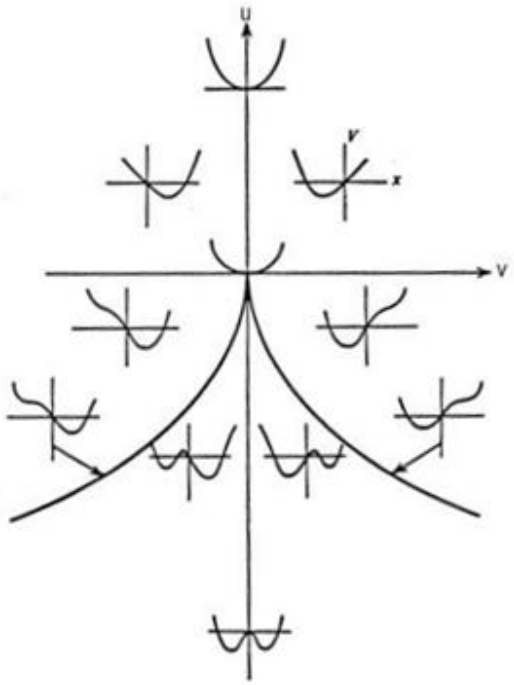

Figure 3.1.2.1 Cusp potential at different values of the control parameters [22]

3.2 Mechanism of energy recovery

Human saves about 80% full mechanical energy while running at any speed. The portion of energy, saved by transferring it between the links of the body, increases significantly and decreases energy transfer due to the transition of kinetic motion energy into the potential in the field of gravity and back with the growth of movement speed.

This is the energy recovery effect that determines the mechanical efficiency of human movements. It is currently believed that saving and reusing or recuperating of mechanical energy occurs through action of three followed mechanisms:

1. Kinetic energy transition into the potential energy and back;
2. Mechanical energy transition or transmission from one link to another;
3. Kinetic movement transition into the potential muscle and tendon deformation energy and back.

First recovery mechanism.

Conservation of total energy by this mechanism requires strictly antiphase change of kinetic and potential fractions of energy. This phenomenon is not observed in all parts of the body. For example, potential and kinetic energy of the foot simultaneously reach zero values in stance phase during walking and running. The link can save more energy if it will be placed higher it over the support base. It is considered, that the first energy recovery mechanism provides energy saving in the range of 12-23% in vivo locomotions in general.

Second recovery mechanism.

Mechanical energy can be transferred from one human body link to another through the exposure articular joints by means of contact forces executing work on changing the energy of the neighboring link. It is reasonable to say about the translational movement energy transition, when force (consistent vertical loading) applied to plateau is converted due to tibia spiral anisotropy and due to special hinge

joint into its rotational energy motion. According to different estimations, energy transmission mechanism from link to link ranges from 30 up to 42% of total energy.

Third recovery mechanism.

Since human muscles only work on reduction, movement in the opposite direction precedes the main movement. Muscle strain in such preliminary movements leads to the accumulation of energy of the elastic deformation in them, which will be used then in the main movement. To be completely accurate, muscle tendon structures are subjected to that stretching. Degree of elastic strain energy use depends on movements performing conditions, in particular, on the time between stretching and shortening of the muscles. Energy efficiency decreases with increasing pause between preliminary stretching and subsequent shortening due to muscle and tendons relaxation. The time interval for which energy must be accumulated and be used for elastic deformation is determined by relaxation time constant, for example, for the knee joint flexion, it is equal to 1.4s. If the movement time is longer relaxation time, stored energy completely dissipates and subsequent phase of the movement is carried out only due to metabolic energy of muscle contraction. According to various sources, recovery energy in the muscle tendon structures range from 6% to 37% [14].

The recuperation effect can be described with the use of Van der Pol equation. The van der Pol oscillator is a non-conservative oscillator with non-linear damping. Energy is dissipated at high amplitudes and generated at low amplitudes. As a result, there exists oscillations around a state at which energy generation and dissipation balance [23].

The Van der Pol oscillator is described as following:

$$\ddot{x} - \mu\left(1 - x^2\right)\dot{x} + x = 0 \tag{3.2.1}$$

and equivalent to the autonomous system:

$$\begin{aligned} \dot{x} &= y - F\left(x\right) := y - \mu\left(\frac{x^3}{3} - x\right) \\ \dot{y} &= -x \end{aligned} \tag{3.2.2}$$

Self-oscillations in such generators are set as follows: small oscillations accidentally occurred in the LC-circuit through the coil L control lamps anodic current, which (with a corresponding mutual arrangement of L and L') amplifies oscillations in the circuit. The amplitude of oscillations increases if the losses in the circuit are less than the energy introduces into the circuit in this way [27].

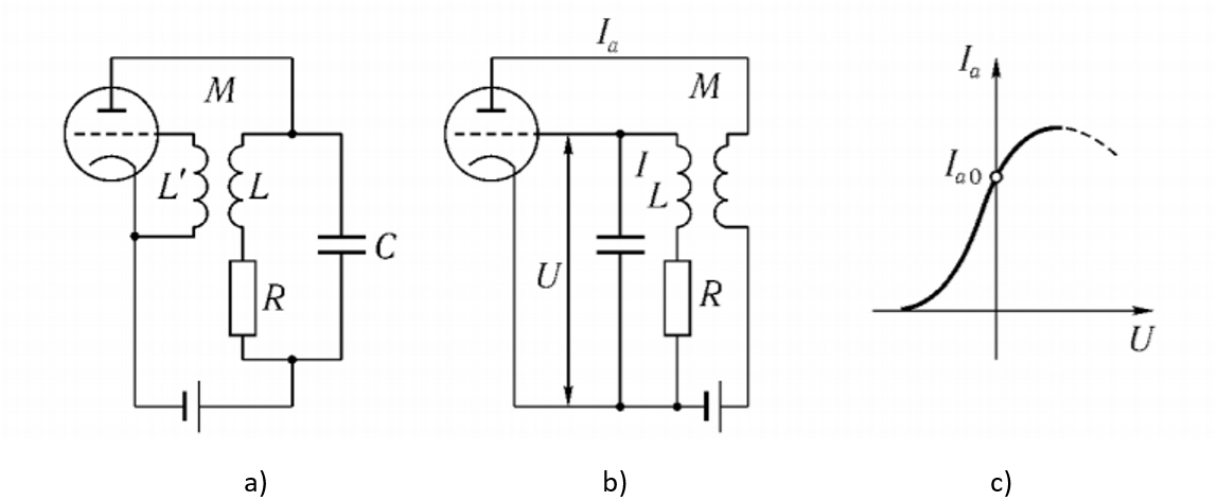

Figure 3.2.1 Van der Pol generator schemes: a – with contour in the anode circuit; b –with contour in the grid circuit; c – lamp characteristics. approximated by a cubic polynomial [27]

With an increase of oscillations' amplitude due to the nonlinear dependence of the anodic current on the voltage on the grid of the lamp, the energy entering the circuit decreases and at a certain amplitude of oscillations is compared with losses. As a result, a stationary periodic oscillation mode is established, in which the anode battery compensates for all energy losses. Thus, in order to establish self-oscillations, nonlinearity is fundamental, which controls the flow and energy loss of the source. Frequency characteristics of the source do not play a crucial role [15,26].

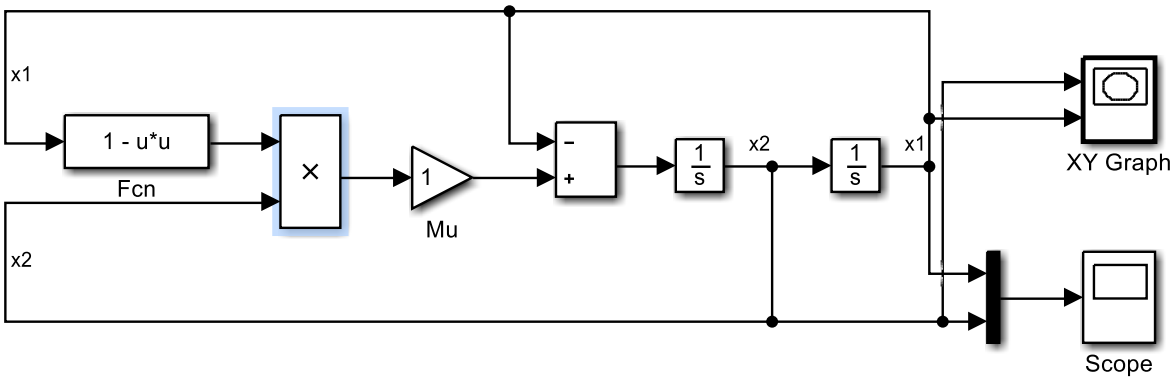

Figure 3.2.2 Van der Pol equation model in Simulink [12]

Phase portrait is shown on Figure 3.2.3.

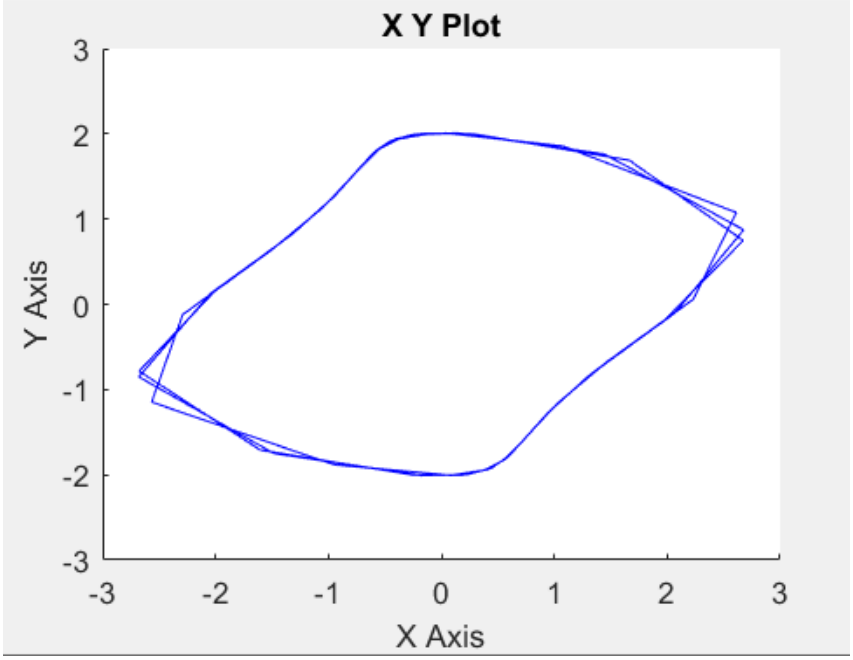

Figure 3.2.3 Phase portrait of Van der Pole equation

Van der Pol equations have found wide application in modeling processes in the human body. The movements of people and animals, such as walking, running or swimming, are known to be carried out in rhythmic, synchronized movements. Coordination of movements occurs in the central nervous

system, which generates signals in accordance with the desired trajectory of movement. The signals are generated by a so-called route generator, which is a network of interconnected non-linear oscillators. Each trajectory of motion corresponds to a certain set of parameters and a certain degree of “connectedness” between oscillators [8].

It was experimentally established that human uses about 200 options of movement during walking. Simulation of such move is possible only due to a significant reduction in the considered options. Figure XX shows a three-dimensional model that covers the most important gait states.

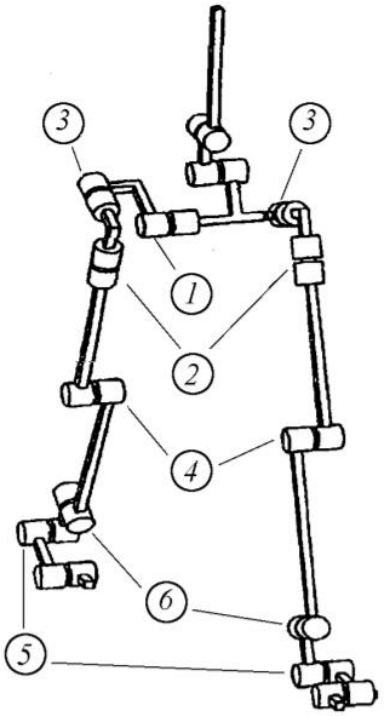

Figure 3.2,3 Three-dimensional model characterized by six major states determining walking [11]

The movement of people and animals is rhythmic, and therefore the control systems of the musculoskeletal system must create rhythmic, synchronized movements of different parts of the limb. Such control systems should also change the frequency, amplitude and phase of movement depending on the gait. A set of coupled non-linear van der Pol oscillators is used as a “route generator”. It is

possible to model bipedal motion using interconnected van der Pol oscillators. By changing the parameters of these oscillators, one can obtain modulation of the stride length and gait frequency [11]

3.3 Knee joint kinematics and dynamics

During the walking cycle the tibia bone rotation varies from +4 degrees to -4 degrees, while the flexion-extension angles varies from 0 to 30 degrees. The +4 degrees value corresponds to the heel strike at the initial contact of the leg with the supporting surface, and -4 corresponds to the end of the contact. Further modeling of the dynamics allowed us to catch the tendency of the interaction of the indicated links without taking into account the obvious cubic nonlinearity. This is the path to evaluate recuperative properties of the system [24].

y - flexion/extension angles (deg);

b - the angle of tibia rotation (deg);

a - parameter.

Figure 3.3.1 demonstrate the patterns of changing y(b) for: a=-9 - solid line; a =-5 - dashed line; a =-2 - dash-dotted line.

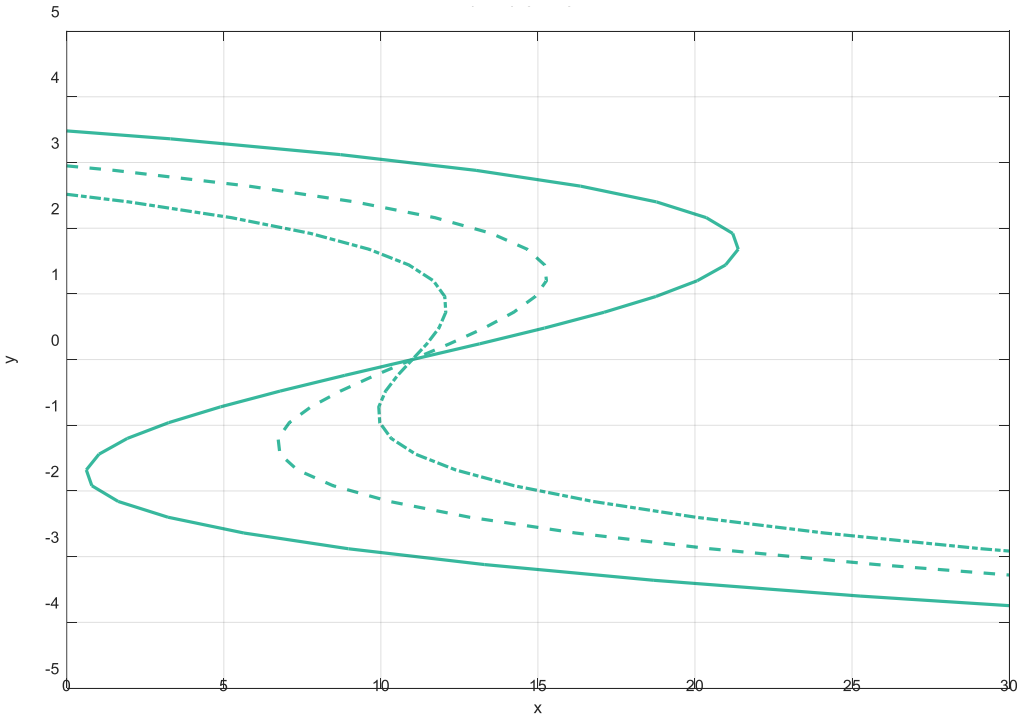

Figure 3.3.1 The patterns of changing y(b)

Dependence obtained for experimental data is:

$$y^3 - ay + (b - 11) = 0 \tag{3.3.1}$$

In the canonical generalized representation sets the two-dimensional manifold, which located in three-dimensional space with coordinate axes y-a-b:

$$y^3 + ay + b = 0 \tag{3.3.2}$$

The solutions of this equation are the critical points of the cusp catastrophe.

$$A(y; a, b) = 1/4\,y^4 + 1/2\,y^2 + by \tag{3.3.3}$$

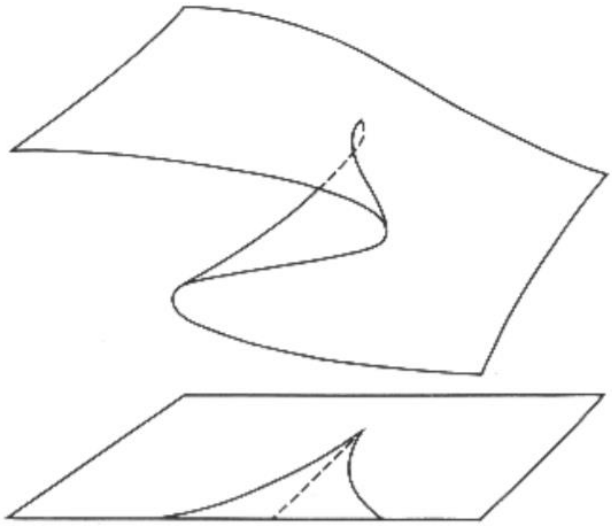

Figure 3.3.2 Cross-section of the cusp [3]

The Figure 3.3.2 curve is a cross-section of the cusp and gives us the basis for the transition to the construction of the dynamic system, which movement is displayed on Figure 3.3.2 when:

$$Fy(y) = y^3 + ay(a < 0) \quad \text{for} \quad b - F(y) \approx 0, \tag{3.3.4}$$

Which follows from the equations of the dynamical system:

$$\begin{aligned} dy/dt &= \gamma\left(b - F(y)\right), \\ db/dt &= -y/\gamma. \end{aligned} \tag{3.3.5}$$

where γ - is damping intensity.

It follows from here that the dynamic behavior of the tibia-femur contact system is characterized by a closed loop trajectory, which is called relaxation oscillation. The circular frequency is approximately taken equal to the one: w=1, hence the cycle period is determined with:

$$T = 2\pi/\omega \rightarrow T = 2\pi \tag{3.3.6}$$

The radius square of this cycle is calculated as follows:

$$R^2 = -4a/3 \quad (a < 0), \tag{3.3.7}$$

That allows us estimate the energy of the system using the stiffness of the contact and then calculate the action transmitted per cycle.

$$J = -2\pi C 4a/3 \tag{3.3.8}$$

Let the actual motion of the system be described by generalized coordinates:

$$q_1(t), q_2(t), \ldots, q_n(t), \tag{3.3.9}$$

The Hamilton action over a period of time (t_1, t_2) is called S, determined by the following expression [7]:

$$S = \int_{t_1}^{t_2} L dt \tag{3.3.10}$$

Where $L = T - V$ is the Langrangian (T – kinetic energy, V – potential energy). Thus, the Hamilton action is a functional.

$T + V = h = const$ - energy conservation law.

Dissipative systems:

$$S = S_1 + iS_2 \tag{3.3.11}$$

$$p(1) = \frac{\partial S_1}{\partial q}, \qquad p(2) = \frac{\partial S_2}{\partial q} \tag{3.3.12}$$

Each generalized coordinate is assigned two generalized impacts

$$q \to \begin{cases} p(1) \\ p(2) \end{cases} \tag{3.3.13}$$

The S value is determined by the choice of n functions of the time $q_1, q_2, \ldots, q_n,$, since L is function of $q_1, q_2, \ldots, q_n, \dot{q}_1, \dot{q}_2, \ldots, \dot{q}_n, t$. In any way when $q_1, q_2, \ldots, q_n, \dot{q}_1, \dot{q}_2, \ldots, \dot{q}_n$ corresponds to a movement, the S action has a certain numerical value [7].

Two quantum axioms are added to quantum mechanics:

$$\int pdq = h\nu \tag{3.3.14}$$

$$h\nu = E_1 - E_2 \tag{3.3.15}$$

where $h\nu$ is frequency radiation.

Formula 3.3.13 determines the stationary states of the atom and characterizes them with an integer n;

Formula determines the radiation.

Returning to the phenomenon of the tibial rotation it is necessary to pay attention not only to the kinematic connection of the joints, but also to the physical and mechanical structure of the tibia, which can be modeled by an elastic equivalent spiral-anisotropic rod, which twists-spins under the longitudinal tension-compression.

On the one hand, it provides energy recuperation. On the other hand, it provides a direction for the construction of recuperation elements in robotic systems.

In addition, as a measure of recovery, it is natural to use the action per walk cycle. Thus, the dynamic system of the knee joint is an oscillatory system and these features should be taken into account during the design of the biomechatronic and robotic systems.

3.4 Enumerative combinatorics

3.4.1 Morse Polynomials.

To distinguish the functions and the Morse polynomial, we designate polynomials by the letter P. The point x0 is called the critical point of the polynomial P=p(x), if it is the root of the polynomial derivative $p'(x_0)=0$. The tangent to the graph of the polynomial at the critical point is horizontal.

The $p(x_0)$ value of the polynomial P at the critical point is called the critical value of this value. A polynomial is called Morse, if:

- all its critical points are real and different:
- all its critical values are different.

Morse polynomials can be described by the following function:

$$P = a_0 x^{n+1} + a_1 x^n + a_2 x^{n-1} + \ldots + a_n. \quad (3.3.1.1)$$

The Morse polynomial of n+1 degree has n critical points and n critical values. We will consider a polynomial of the form:

$$P = x^{n+1} + a_1 x^n + a_2 x^{n-1} + \ldots + a_n. \quad (3.3.1.2)$$

where the leading coefficient is 1 ($a_0=1$).

Each Morse polynomial corresponds to a specific numeric sequence (transposition), the amount of numbers in which is determined by the number of critical points in this function (by the n value). This transposition indicates the order in which the critical values of the polynomial follow.

Transpositions are formed according to the conditional rule: first, the critical points are numbered in ascending order of the critical function values, and then the numbers are collected from the smaller values along the abscissa axis towards the larger values [19].

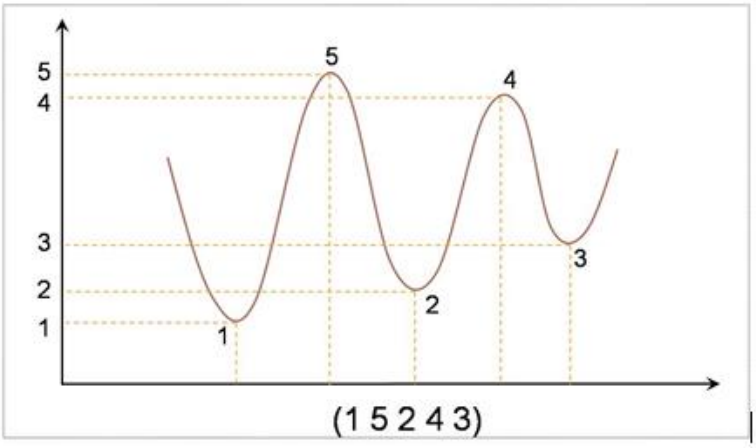

Figure 3.3.1.1 The rule for finding the transposition of polynomial n=5 [19]

Such transpositions are called saw tooth or up-down transpositions. The saw tooth transposition corresponding to the Morse polynomial is called the type of this polynomial.

Notice, that not any saw tooth transposition can serve as a type of Morse polynomial, but only that, the last critical value of which is less than the previous critical value. As a result, for polynomials with odd number - n, the first element in the transposition must be less than the next element, with an even number - n - the first element is more than the next element.

Based on the above rule, Morse polynomials can be divided into two groups:

- if n is odd (n=1,3,5,7,...), the last elements are bigger its neighbors, and these polynomials are called odd [y1 < y2 > y3 < y4 > y5 …]; Figure 3.4.1.2
- if n is even (n=2,4,6,...), the first elements is always greater than the second, and such polynomials are called even [y1 > y2 < y3 > y4 < y5 …]. Figure 3.4.1.3

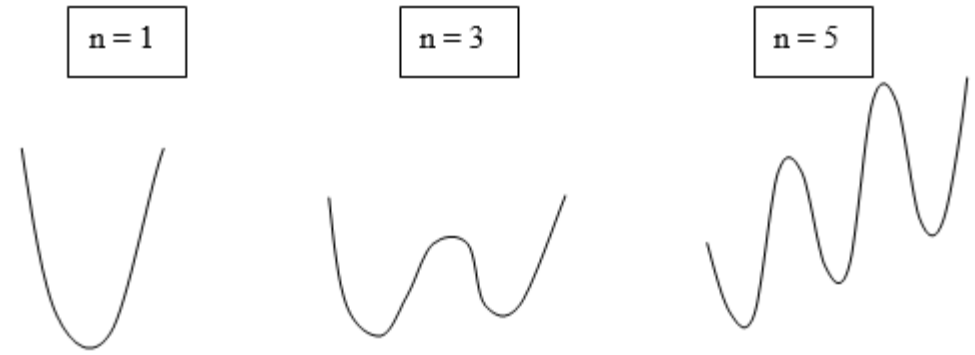

Figure 3.4.1.2 Odd Morse polynomial

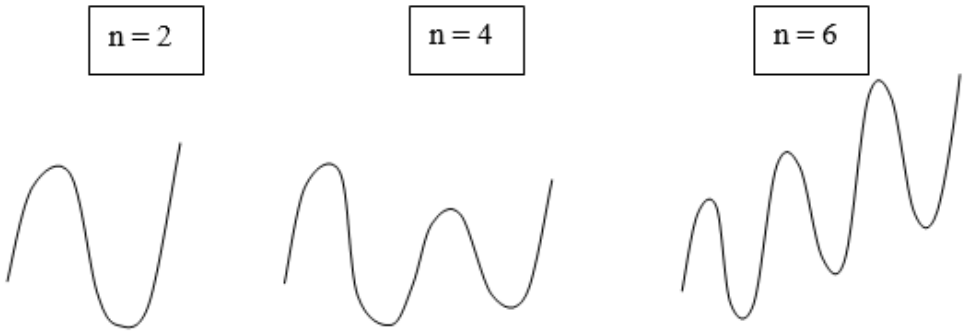

Figure 3.4.1.3 Even Morse polynomial

Enumeration feature description of Morse polynomials.

The types of Morse polynomials for small n values are shown on Figure 3.4.1.4. For n=1 and n=2 there is only one possibility. With n=3 there are two possibilities, with n=4 such opportunities five.

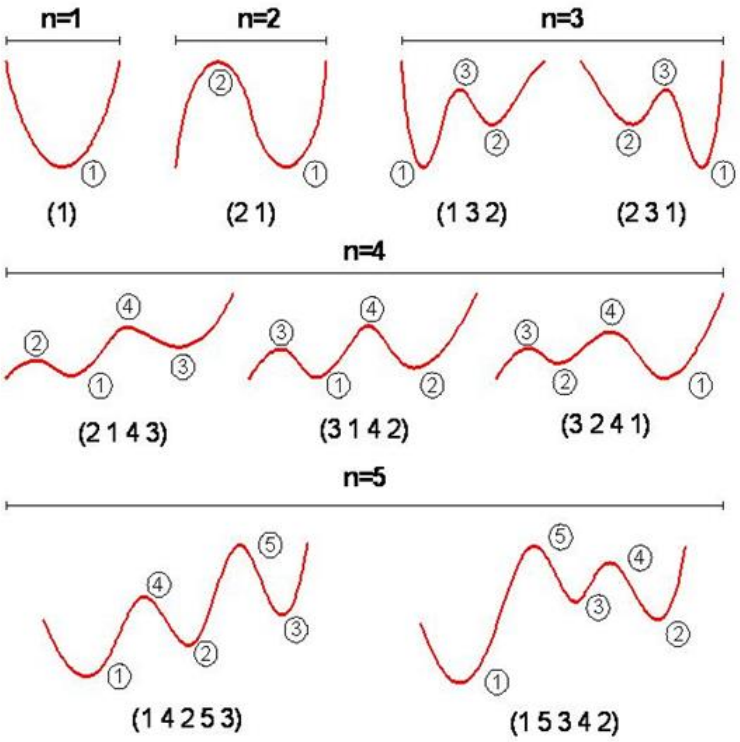

Figure 3.4.1.4 - Transposition options for different Morse polynomials.

If we continue the listing of possibilities, we can obtain the sequence:

1, 1, 2, 5, 16, 61, 272, …

3.4.2 Algorithm and program for finding the Morse polynomials and calculating critical points and critical values

If the third-degree polynomial coefficients (n=2) can be chosen by substitution so that the roots of the derivative are real (which is a necessary condition for the existence of the Morse polynomials), then for fifth (n=4) and higher degrees it is advisable to create a special program that automates the search for real roots. MATLAB programming platform was chosen as programming environment.

The task of the program is to find the maximum possible number of type n=4 Morse polynomials, calculate all parameters, i.e, the equation of the function itself with satisfying coefficients, the coordinates of their extremes and graphical output of results.

The defined polynomial transposition and intervals of enumeration of coefficients with given step are entered from the keyboard to the program. The first important condition for the existence of polynomials is the real root of its derivative. Polynomials that satisfy the following condition go to the next stage of the program.

$$P = ax^5 + bx^4 + cx^3 + dx^2 + ex + f \tag{3.4.2.1}$$

$$P' = 5ax^4 + 4bx^3 + 3cx^2 + 2dx + e = 0 \tag{3.4.2.2}$$

To simplify calculations, coefficient a=1 is applied (it only affects the scaling of the function itself) b coefficient g=0 (it only affects the offset of the function without changing its shape).

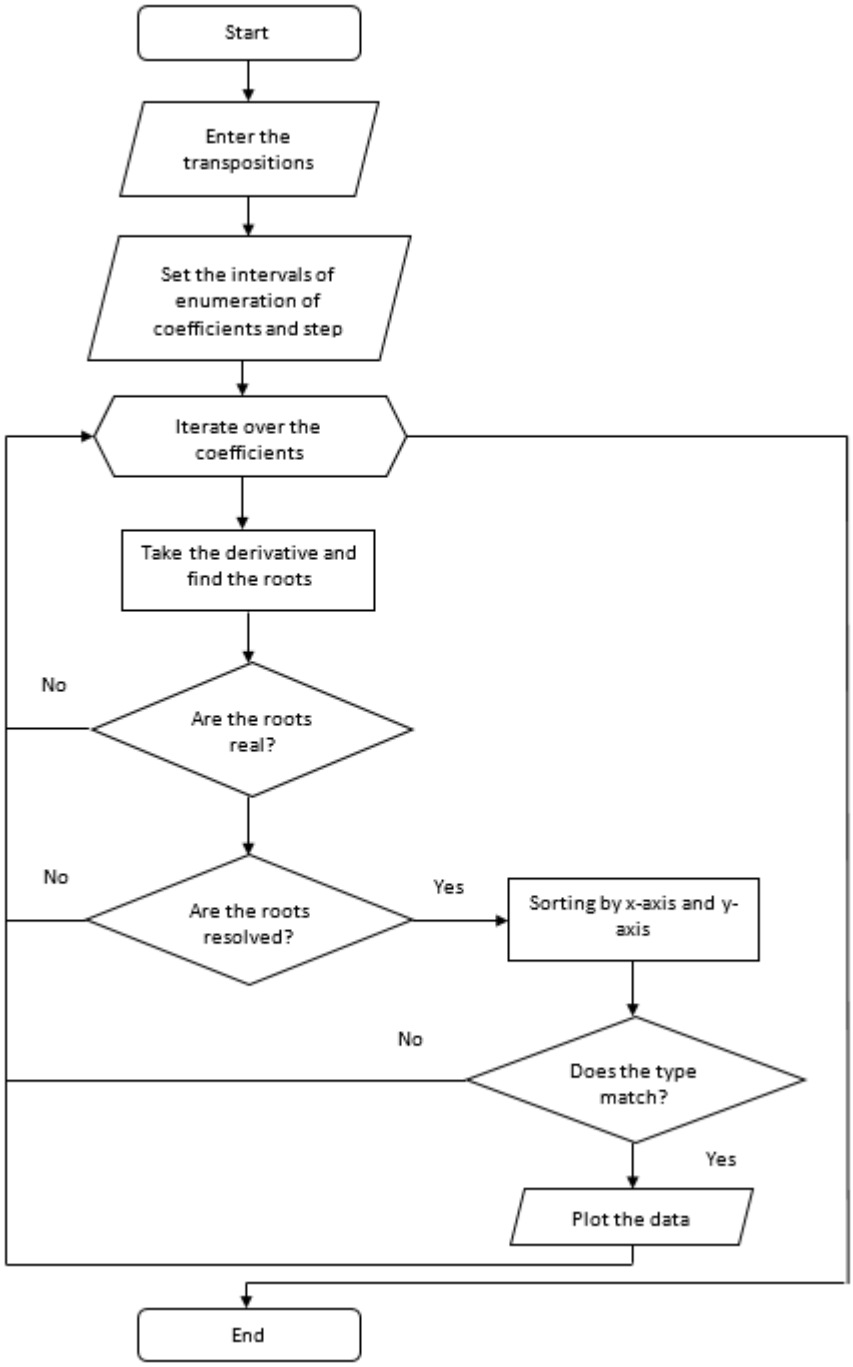

Figure 3.4.2.1 Algorithm of the program [19]

The second important criterion is the inequality of the roots; when it is executed, the polynomials become Morse. Finally, if both conditions are met, the roots are sorted in ascending order, and the corresponding values are calculated along the abscissa axes. After that, we can find out whether the

obtained Morse polynomial satisfies the transposition given at the beginning of the program. If the desired transposition is found, the program proceeds to the stage of graphical output of all characteristics.

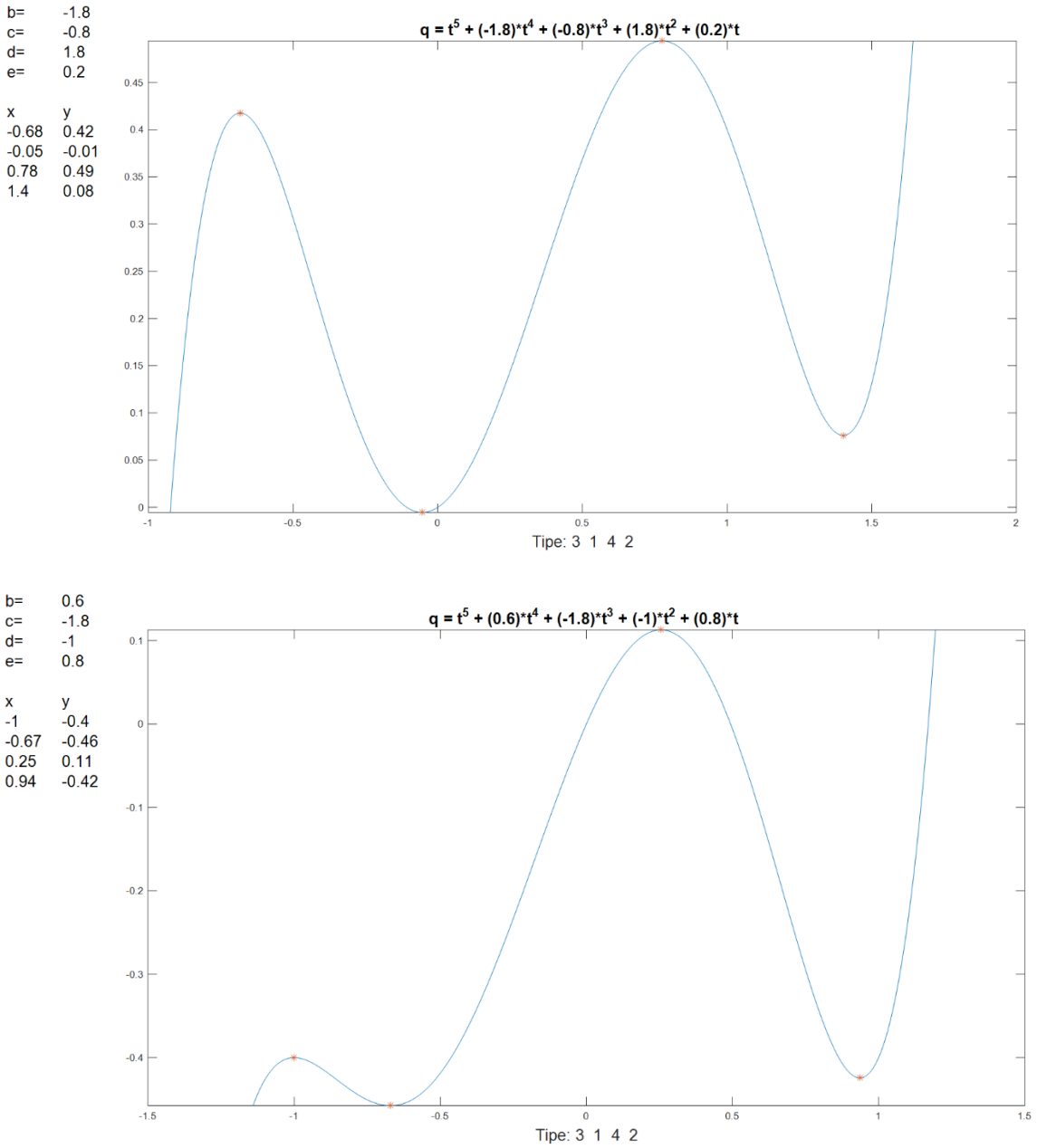

Figure 3.4.2.2 An example of the program results for finding Morse polynomials corresponding to the transposition (3 1 4 2)

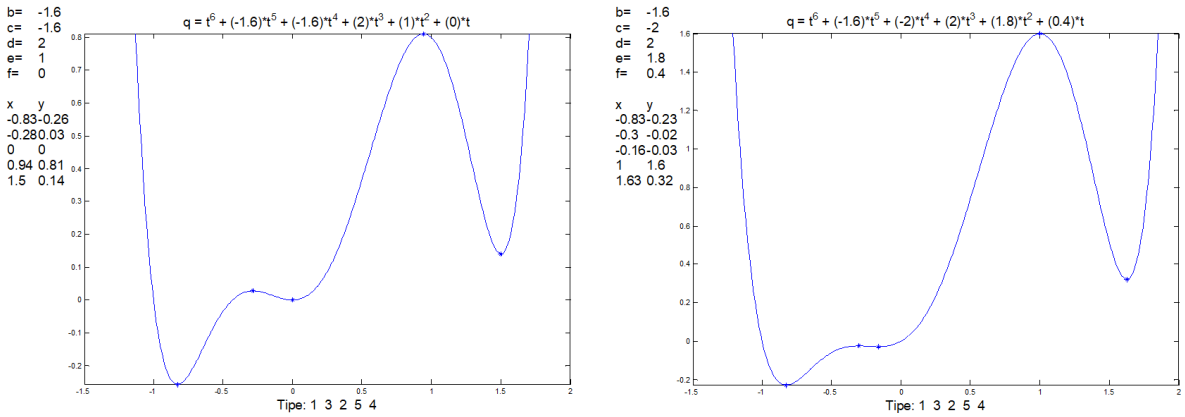

Figure 3.4.2.3 An example of the program results for finding Morse polynomials corresponding to the transposition (1 3 2 5 4)

The figure shows the results of the work of such program, in which we can see the same transposition with different characteristics. The function that describes each particular polynomial is displayed above the graph. An array with selected coefficients and extremum coordinates is formed to the left of the graph. Along with a graphical output, a text file for each maximum and minimum, containing the same parameters as in the graph is generated.

The similar method could be used for finding Morse polynomials with n=5, 7, 9, … . But this method turns out to be practically inapplicable, since here we find polynomials by enumerating the coefficients. We set the values of the coefficients up to the tenth, and this is enough for us to get a sufficient number of polynomials of a given type. When the degree of polynomials increases, the coefficients become more complex and, in most cases, irrational, so it is difficult to find their values using the sorting method. In this case, it is advisable to approach this task from the other end and look through the critical values of polynomials themselves. Here, the condition of checking the roots for validity disappears, which rationalizes the operation of the program. The coefficients themselves are already calculated depending on the combination of the found roots.

3.4.3 Allocation sequence numbers of critical values in the transpositions

Morse polynomials with n-5 are considered. All polynomials of this group have three “minima” and two “maxima” alternating with each other. V1, V2, V3 denote the “minima”, and λ1, λ2 – “maxima”, as shown on Figure 3.4.3.1.

This type of polynomials has 16 transpositions, and it is possible to determine the frequency of occurrence of the sequence numbers of extremes (1. 2. 3. 4. or 5) at the position of a particular minimum” or “maxima”.

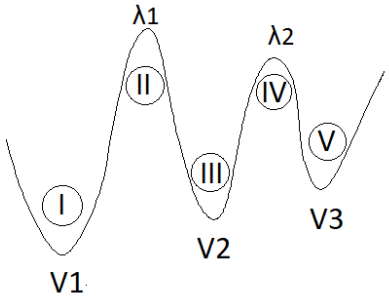

Figure 3.4.3.1 Denotation “maxima” and “minima” of the polynomials

3.4.4 Distribution of critical points and critical values of Morse polynomials

The Morse polynomial of type (3 5 2 4 1) is considered. In the process of the previous program, aimed at finding the same type of polynomials, going through the coefficients of the polynomial on the interval [-2;2] with step 0.2 224 different polynomials, with spreading the extreme coordinates in some areas were found, however, what is important, of the same type.

The function’s first bend is considered (first minimum). All received value of the first critical point are guaranteed to fit into a gap resulting during calculations. This gap is divided into a number of equal parts. With the help of a MATLAB and *histfit* command, from a formed file with critical points and critical values for the first extremum, histogram of the probability of hitting the first critical point in each of the areas inscribed in the law of the normal Gaussian distribution is displayed on the screen. The same

procedure is repeated to find the distribution of critical values corresponding to the critical points of the first extremum.

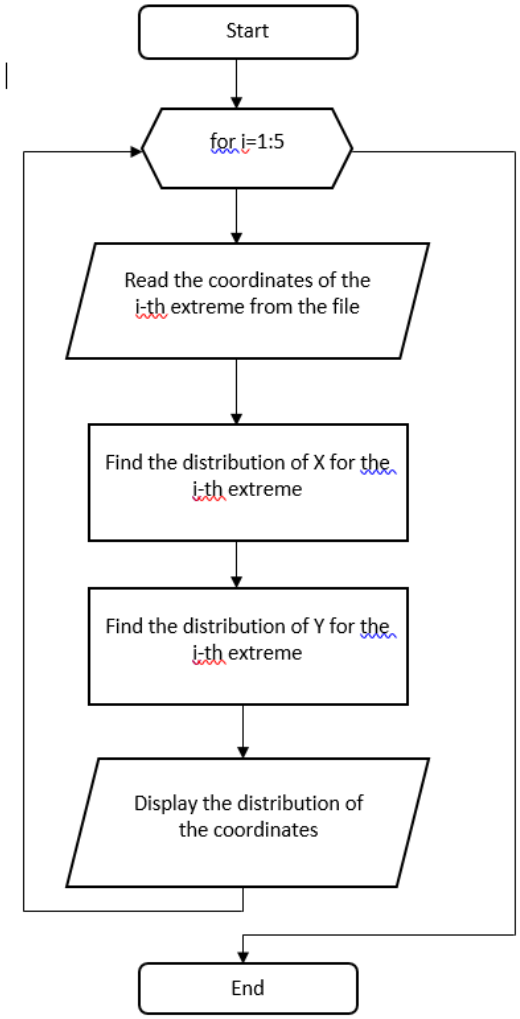

Figure 3.4.4.1 Algorithm of finding the distribution of critical points and values [19]

A sample of the program is presented in the appendix.

On the figure 3.4.4.2 two graphs are near the first extremum, the lower of which corresponds to the distribution of critical points, and the upper one – of critical values. Similar actions are performed for the remaining maxima and minima of the function and are summarized on the general graph.

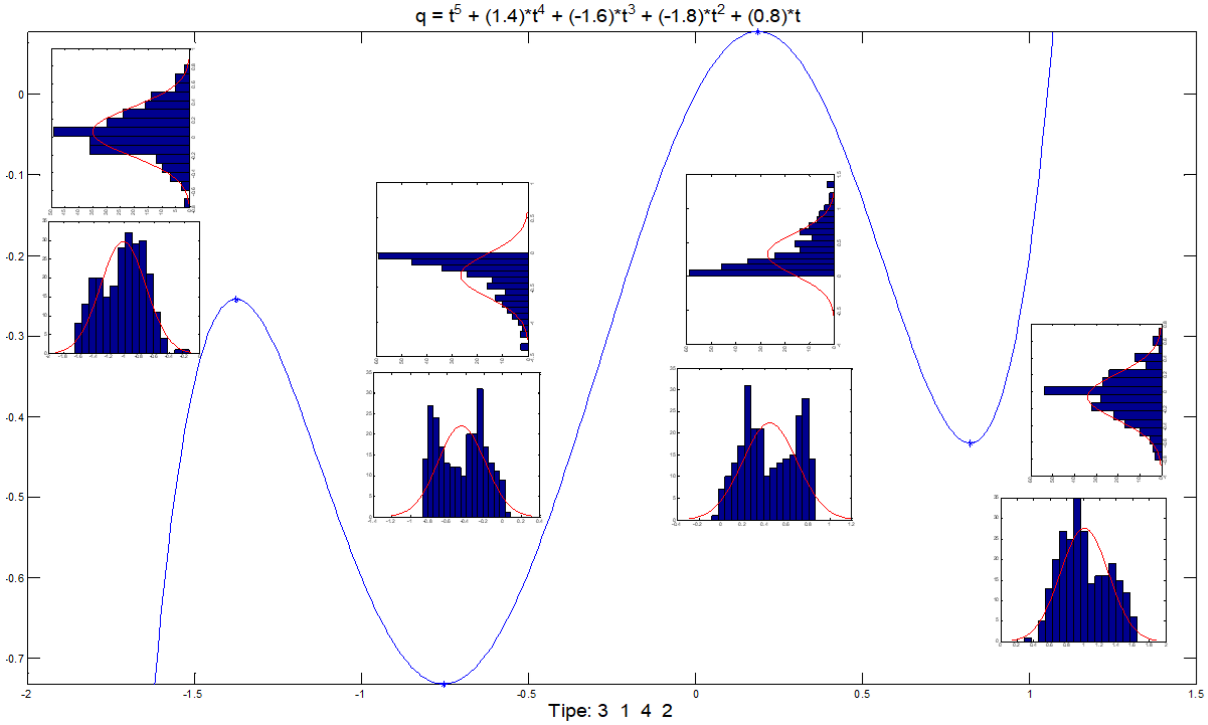

Figure 3.4.4.2 The distribution law of critical points and critical values of the Morse polynomial for even polynomials

3.5 Conclusion

In this chapter, the theoretical foundations for further mathematical modeling of human walking was reviewed.

The model of the knee rotation during walking is effectively described by the equation of the cusp catastrophe. Energy recovery in the knee joint is represented in the mutual transitions of torsional and bending modes.

To simulate the kinematics of the extension and rotation of the knee, the best results were obtained using Morse polynomials. The proposed program algorithm finds the coefficients of the corresponding transpositions.

4. Human walking experiments conducted in Tartu University

4.1 Obtaining experimental data

Research work is based on the experiments conducted in the Laboratory of Kinesiology and Biomechanics of the University of Tartu, which was founded in 1968 on the basis of the Institute of Sport Sciences and Physiotherapy.

Today the laboratory has one of the newest measuring equipment: Italian-made podobarometer, a center of mass distribution platform, wireless electromyography sensors for studying electrical muscle activity, an optical marker system for motion capturing, etc.

The Tartu University Laboratory is a member of the EU 7RP Project MYOAGE international research group. Their main modern projects are: "Understanding and combating age-related muscle weakness - MYOAGE", EU FP7 project and ("Myoton Literate for muscle target scores - MYOLITE "EU EUREKA Eurostars program [16].

Internal laboratory studies are focused on:

- the investigation of various diseases in athletes which occur in the muscular and motor apparatus due to the long training practices;
- the study of the influence of different external factors on the physiology of athletes;
- the study of children and adults with diseases of the musculoskeletal system; pre- and postoperative periods of patients with osteoarthritis are observed.

The task of the experiment is to track the fragments constituting the bodies of the MSS.

Experimental data were received with this type of equipment:

- optical marker system;
- goniometers;
- wireless electromyographs;
- static pressure platform;
- center of mass distribution platform;
- G-WALK.

Four women aged 22-28 (mean ± SE, body mass 64,6 ± 4,3 kg, height 166,8 ± 3.4 cm and body mass index 23,2 ± 1,0 kg / m2) without any health problems, who had no history injuries, no surgeries and other pathologies of the musculoskeletal and nervous system, who were not professional athletes were involved in the study. Kinetic and kinematic characteristics of the gait were investigated using the Elite Optoelectronic Motion Analysis System (BTS Engineering S.p.A., Italy) [6].

Optical marker method of motion capture and analyzing was chosen as the main research method. The basis of this method is camera-sensors installed along the space area perimeter where capture occurs.

Optical markers consist of retro-reflective material, which reflects incoming infrared light back into the light source. Such markers are available in different sizes as flat, round stickers, or in a spherical shape. Spherical markers have the advantage that they reflect light in all possible directions with respect to the tracking system, whereas flat markers only reflect light at an angle between 0 and 60 degrees wit respect to the tracking system. In our experiments special silver round markers were fixed on the human body, during the movements in the area recorded by the cameras [6].

Markers are placed on the body of the subject according to the standard model presented on Figure 4.1.1. Qualified medical personnel carry out the attachment of the markers.

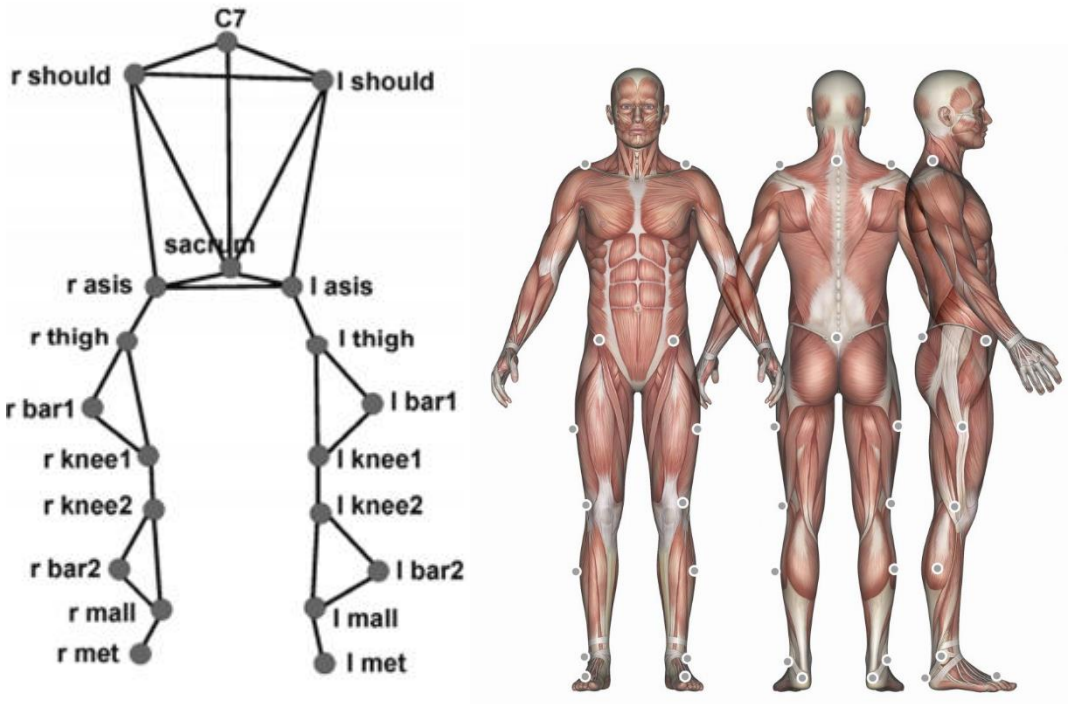

Figure 4.1.1 Biomechanical model of torso and lower extremities [6]

6 Infrared cameras are placed along the perimeter of the room, separate block register their signals and transfer them to the software for processing and receiving the animated model.

Equipment:

- 6 cameras;
- 20 markers;
- recorder (computer with converter)

Software:

- for processing signals from cameras and creating the models;
- for data analyzing and plotting;

The center of mass distribution platform is part of an integrated motion analyzing complex along with an optical marker system. The platform consists of two sensitive units, the signal, representing the mass distribution during movement, the force of pressure on the platform, as well as the direction of the total motion vector, is recorded during the movement along those units.

The load is perceived by the strain gauges of the platform and is converted into an electrical signal. The registration of the dynamic characteristics of walking is performed simultaneously with the motion capture of the marker biomechanical model of the body.

Processing and plotting takes place in the tasks are done by a special software. Both methods allow us obtain data on kinematics and dynamics of human walking.

The laboratory also has a podobarometric platform for recording the distribution of the foot pressure. The systems consists of a large number of sensors (4 sensors per centimeter) uniformly distributed over the platform. As a result, the software visualizes data of the foot area pressure distribution; returns the values of the foot area; maximum and minimum pressure values; the balance ratios on the right and left legs; calculates the center of gravity of the subject's body, as well as the equilibrium centers for each foot.

Geometric parameters of patient body segments were measured by anthropometric methods before conducting static tests on the podobarometer platform and kinematic studies in the optical marker system. The main parameters are height, weight, leg length from the hip to the floor, length of the thigh, lower leg, pelvis width and height of the pelvic bones, diameter of the knees and lower leg [6].

During the experiments optical marker system and static pressure platform were used.

Tests were conducted for two paces of walking: normal and fast. For statistics, each pass is repeated three times. An important part of the experiments is the need to double step on the center of mass distribution platform during the passage, i.e. make a full step on it.

After receiving data from cameras to the software, the construction of the kinematic model by marker points begins.

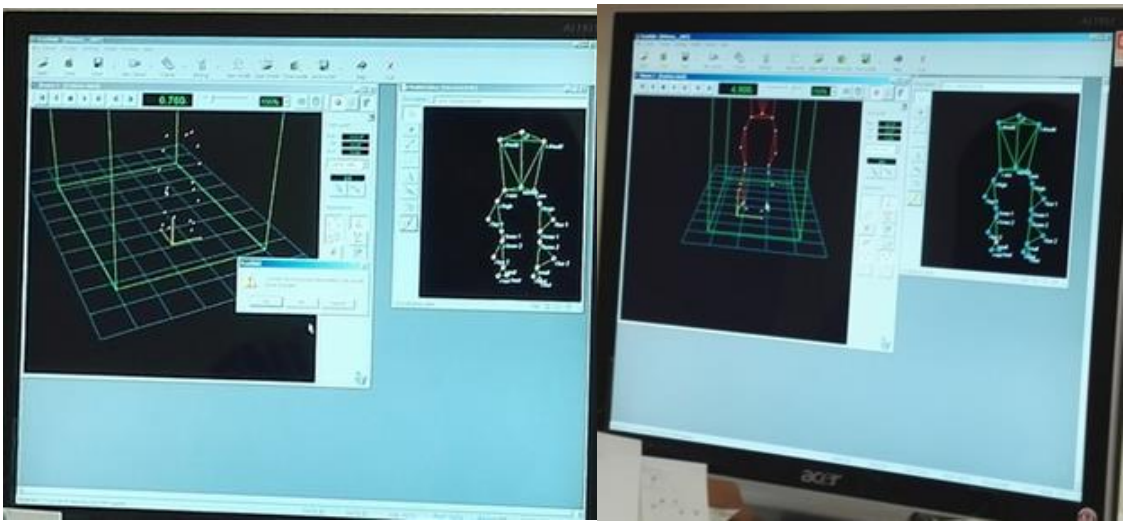

Figure 4.1.2 Building the kinematic model from the cameras.

Based on the constructed model and data set from the recorder, program plots graphs of the dependencies of the bend angles for each leg; pelvis bones movement and rotation; hips, knees, lower legs moments and power (muscular effort) are calculated; and also correlated with the step cycle support reaction graphs are constructed: heel forces, medial-lateral forces, forces in the vertical direction.

4.2 Experiment results

Anthropometric parameters measured during the study for four subjects (B, M, P, A), are presented in table 4.2.1.

Table 4.2.1 Anthropometric data of the examined B, M, P, A [18]

Parameter	Examined subject			
	B	M	P	A
Age, years	28	22	28	26
Mass, kg	70,5	56,1	73,45	58,4
Height, cm	169,9	157	172,3	168,8
The length of the lower extremities, cm	102	87,5	98,5	100

Thigh length, cm	51,5	44,5	53,5	51,3
Tibia length to the floor, cm	50,5	42,5	45	48,7
Length tibia to the ankle, cm	43	37,5	40	42
Foot length, cm	24,7	23,6	25,5	26,6
Foot width, cm	9,5	9,6	10,7	10,5
Width of the back of the foot, cm	7,2	6,2	6,7	6,4
Pelvis size, mm	90	80	80	80
Constant parameter	0,5878	0,7159	0,3994	0,7095

The indicators were analyzed when walking at a normal pace (freely selected walking speed) on a 10-meter track, including a 5-meter platform located in the center of the system's infrared and video camera registration area. In this study, the kinematic parameters of flexion and extension in the hip and knee joint, based on the average data of five tests at the normal pace of each test were taken to build a walking model.

For the developing of a mathematical model of the movement of the lower extremity it is considered use simplified kinematic scheme of the four-link mechanism with one degree of freedom (Figure 3.1.1) [2].

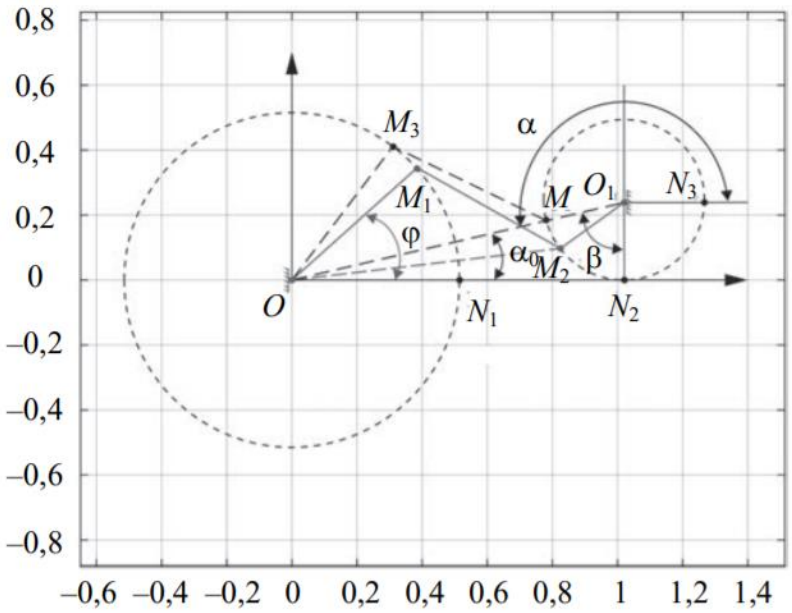

Figure 4.2.1 Four-link mechanism scheme [18]

The following notation is introduced on the presented kinematic scheme.

$OM_3 = OM_1 = l_1$ - thigh length;

$O_1M = O_1M_2 = r$ - foot length;

$M_3M = M_1M_2 = l_2$ - shin length;

L = total shin and thigh length;

φ - hip rotation angle;

α_0 - fixed angle of the kinematic system;

$\beta = \pi/2 - \alpha_0$

α - foot rotation angle;

x_1y_1 - coordinates of point M_1 (current coordinates);

x_2y_2 - coordinates of point M_2 (current coordinates).

Fixed angles of the kinematic system determine, on the one hand, the goniometric parameters, on the other hand, limit configurations of the system before the end of the forefoot push phase or phase of contact "toe-to-ground".

Consider the equations of the system:

Connection 1.

$$Pg = r\sin(\alpha) \tag{4.2.1}$$

projection of the rotating O_1M_2 on the horizontal axis;

$$Pv = r\cos(\alpha) \tag{4.2.2}$$

projection of the rotating O_1M_2 on the vertical axis;

The calculated values of M_2 coordinates are following:

$$x_2 = L - Pg;\ \ y_2 = r - Pv; \tag{4.2.3}$$

$$Pg^2 + Pv^2 = r^2 \to \left(Pg^2 + Pv^2 - r^2 = 0\right). \tag{4.2.4}$$

Connection 2.

M_1 point coordinates:

$$x_1 = l_1\cos(\varphi);\ \ y_1 = l_1\sin(\varphi) \tag{4.2.5}$$

$$x_1^2 + y_1^2 = l_1^2 \to \left(x_1^2 + y_1^2 - l_1^2 = 0\right). \tag{4.2.6}$$

Connection 3.

$$\left(x_2 - x_1\right)^2 + \left(y_2 - y_1\right)^2 = l_2^2 \rightarrow \left(\left(x_2 - x_1\right)^2 + \left(y_2 - y_1\right)^2 - l_2^2 = 0\right). \quad (4.2.7)$$

From connection equations (4.2.4 – 4.2.7) follows:

$$\left(Lx_2 + ry_2\right) - \left(x_1 x_2 + y_1 y_2\right) = R, \text{ where } R = \left(l_2^2 - l_1^2 - L^2\right)/2. \quad (4.2.8)$$

There are two more connections:

$$z_1 = 0;\ z_2 = 0. \quad (4.2.9)$$

Thus, for five connection conditions and two mechanical points (biomechanical) system we obtain a system with one degree of freedom. Equation 4.2.8 is the base for calculating the parameter k.

$$\varphi = k\alpha;\ k = \varphi^* / \beta;\ \beta = \pi/2 - \alpha_0. \quad (4.2.10)$$

The parameter k characterizes the constancy of the OO_1 from the support toe point O_1 to the hip rotating point O and the constancy of the $M_3M = M_1M_2 = N_1N_2 = l_2$. As a result, this parameter, as it should be in a system with one degree of freedom, allowed to connect the rotation angle φ and α by the linear dependence $\varphi = k\alpha$ (counting for α is made counterclockwise along the arc N_3M_2) [18].

The algorithm for calculating the parameter k:

1. Coordinates of the point $M\left(x2_0, y2_0\right)$ are calculated;
2. Function $F = \left(x2_0 - l_1\cos\left(\varphi\right)^2 + y2_0 - l_1\sin\left(\varphi\right)^2\right)$ is build;
3. l_2^2 value is found and the value φ^* is determined form it;
4. The value of the parameter $k = \varphi^* / \beta$ is found.

Figure 4.2.2 shows the schemes of four-linkers corresponding to anthropometric data of the subjects. It also shows the values of the calculated coefficients of constancy k.

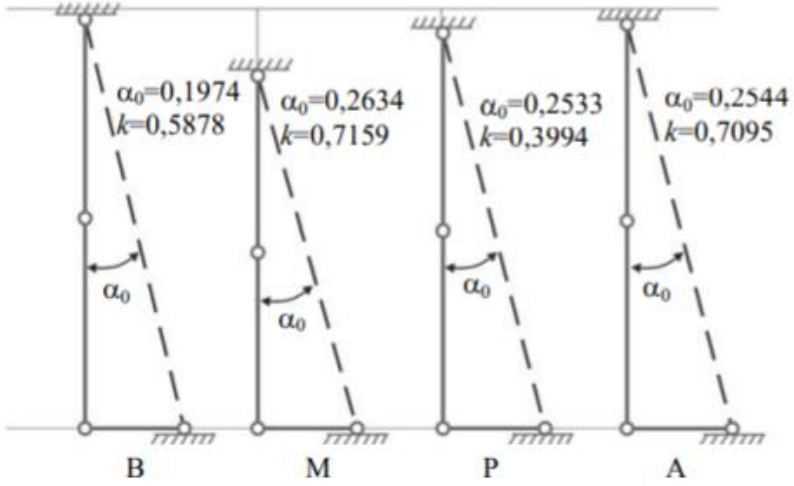

Figure 4.2.2 Schemes of the four-link mechanisms corresponding to anthropometric data [18]

Table 4.2.2 The frequency and amplitude of the basic movement of the joints [18]

Examined subject	G Hip Flex-Extension	M Knee Flex-Extension	R Ankle Dorsi-Plantar
B	$\Omega_1 = 6.97\,Hz,\ A = 21.5$	$\Omega_2 = 15.7\,Hz$	$\Omega_3 = 11.4\,Hz$
M	$\Omega_1 = 7.85\,Hz,\ A = 27.5$	$\Omega_2 = 12.56\,Hz$	$\Omega_3 = 12.83\,Hz$
P	$\Omega_1 = 7.3\,Hz,\ A = 18.5$	$\Omega_2 = 15.3\,Hz$	$\Omega_3 = 14.9\,Hz$
A	$\Omega_1 = 7.22\,Hz,\ A = 20$	$\Omega_2 = 13.08\,Hz$	$\Omega_3 = 11.62\,Hz$

Ω_1 - frequency of oscillations in the hip joint,

Ω_2 - frequency of oscillations of the knee,

Ω_3 - frequency of oscillations in the ankle joint,

A - amplitude of oscillations in the hip joint in relation to a - the amplitude of the slopes of the hip joint

The motion equations in this case are not considered, they are described in detail in the article [18].

4.3 Finding Morse polynomials for experimental data

Among the different graphs, obtained during the experiments, Knee Flex-Extension and R-knee Rotation can be represented as Morse Polynomials. According to the rule of defining the type of the Morse polynomials, described dependence is 3-1-4-2 transposition.

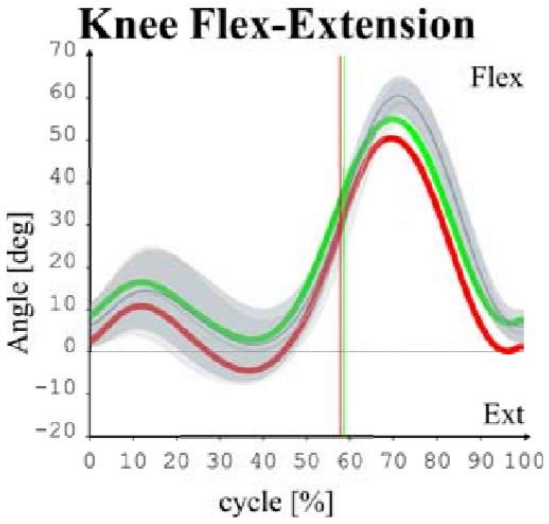

Figure 4.3.1 Knee Flex-Extension diagram [18]

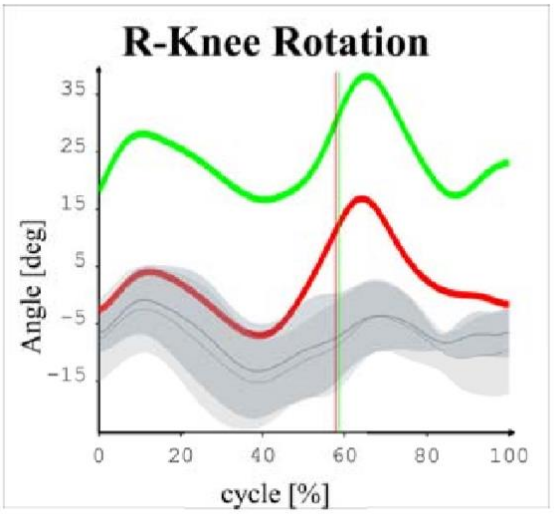

Figure 4.3.2 R-knee Rotation diagram [18]

With the use of the program for calculating the polynomial combinations following results were obtained. The program code is presented in the Appendix.

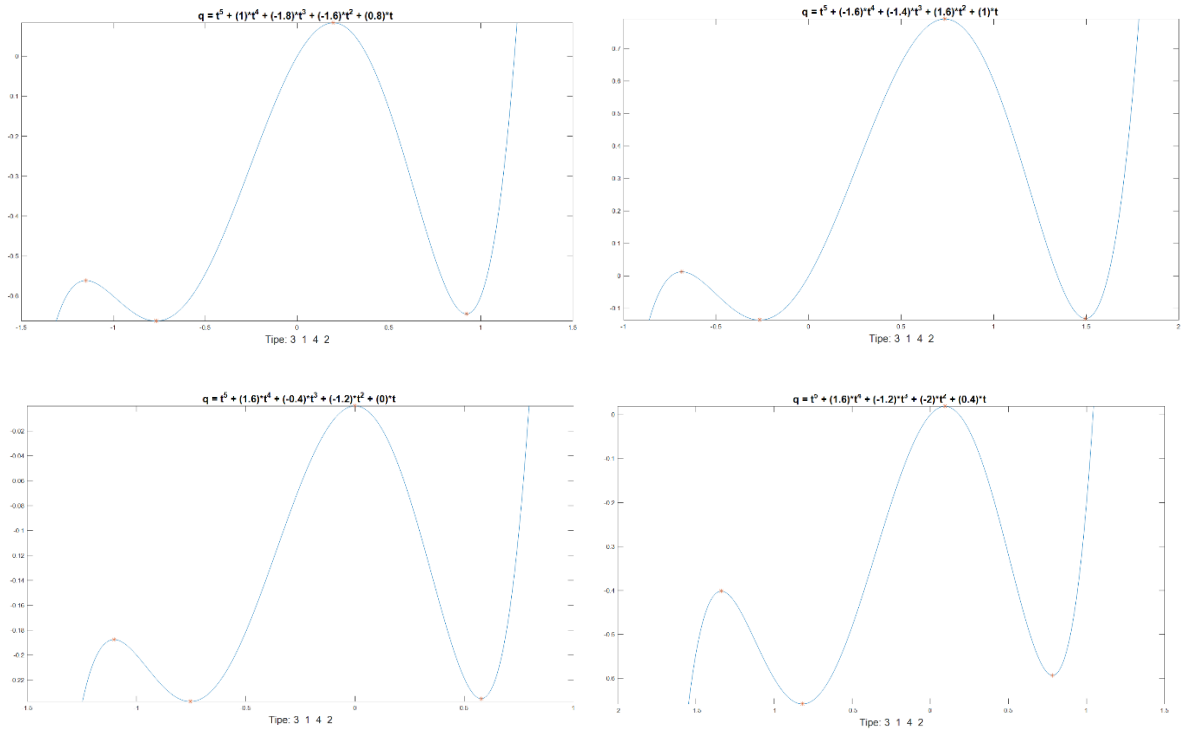

Figure 4.3.3 Found Morse polynomials

As it can be noticed, found polynomials with some enhancement can be used us mathematical model for knee flex-extension dependence.

4.4 Conclusion

This chapter presents the results of experiments conducted in Tartu, as well as an analysis of the results carried out by researchers from Portugal and Japan. A simplified kinematic scheme of the four-link mechanism, corresponding to the anthropometric data of each tested subject is considered. An algorithm of calculating of the constancy coefficient k is presented.

5. SUMMARY

Analysis of work related to the study of the human MSS showed that the most productive hardware means are means of optical fixation and means of inertial technology.

A series of experiments was conducted in the laboratory of kinesiology and biomechanics of the Tartu Classical University to study the kinematics of human movement using optical means (an optoelectronic system for the analysis of movements Elite BTS Engineering S.p.A), as well as a podobarometer platform.

It is shown that the kinematics of motion can be effectively described with the help of Morse polynomials. A program for searching the corresponding polynomials of certain transposition has been developed. In the process, we stopped to consider the kinematics of Knee-Flex-Extension and R-knee Rotation. According to the rule for describing Morse polynomials, this transposition has the form 3-1-4-2. The paper presents the results of the selection of the corresponding transposition.

In order to demonstrate the recovery abilities of the elements of the human musculoskeletal system, based on the research conducted by Ribeiro et al., which was based on the Lafortune et al. experiments, the theory of catastrophes was used. The solution of the equation defining the cusp catastrophe provided the basis for the transition of the construction of a dynamic system of tibial-femoral contact. The dynamics of redistribution of energy was based on the Van der Pol equation.

Results of the study is planned to be used in the analysis of the movement of both healthy subjects and subjects with impaired function of the musculoskeletal system. In particular, the results will be important in the manufacture of an orthosis of the lower extremities, the implementation of the movement of which would fit into the standard of movement of a healthy person.

6. LIST OF REFERENCES

[1] Arnod, Vladimir Igorevich, and Yuliy Sergeyevich Ilyashenko. "Obyknovennyye differentsialnyye uravneniya." Itogi nauki i tekhniki. Seriya «Sovremennyye problemy matematiki. Fundamentalnyye napravleniya» 1.0 (1985): 7-140.

[2] Arnold, Vladimir Igorevich. Matematicheskiye metody klassicheskoy mekhaniki. Ripol Klassik, 1979.

[3] Arnold, Vladimir Igorevich. Teoriya katastrof. URSS, 2007.

[4] Au, Samuel, Max Berniker, and Hugh Herr. "Powered ankle-foot prosthesis to assist level-ground and stair-descent gaits." Neural Networks 21.4 (2008): 654-666.

[5] Beletskiy, Vladimir Vasilyevich. Dvunogaya khodba: modelnyye zadachi dinamiki i upravleniya. Nauka. Gl. red. fiz.-mat. lit., 1984.

[6] BTS motion capture system. Retrieved November 20, 2018 from https://www.btsbioengineering.com/products/smart-dx/

[7] Butenin, Nikolay Vasilyevich, Yuriy Isaakovich Neymark, and Nikolay Alekseyevich Fufayev. "Vvedeniye v teoriyu nelineynykh kolebaniy." NV Butenin, YUI Naymark, NA Fufayev (1976).

[8] Cao, Wesley. "Van der Pol Oscillator." Celestial mechanics, MAT983. Junior Seminar on Hamiltonian Mechanics. 2013.

[9] Davis, Roy B., Peter A. DeLuca, and Sylvia Ounpuu. "Analysis of gait." Biomechanics: Principles and Applications 20 (2002): 131.

[10] DeLisa, Joel A., ed. Gait analysis in the science of rehabilitation. Vol. 2. Diane Publishing, 1998.

[11] Dutra, Max S., Armando C. de Pina Filho, and Vitor F. Romano. "Modeling of a bipedal locomotor using coupled nonlinear oscillators of Van der Pol." Biological Cybernetics 88.4 (2003): 286-292.

[12] Dyakonov, Vladimir. MATLAB 6/6.1/6.5+ Simulink 4/5 v matematike i modelirovanii. Litres, 2018.

[13] Erofeev, Mikhail, Ovcharov, Aleksei and Nurmukhanova Assel. "Using the human walking pattern for the control system of an electromechanical robotic arm." IEEE 2019 International Conference on Mechatronics, in press.

[14] Kolyubin, Sergey, and Viktor Musalimov. "Biomekhatronika: shagi navstrechu energoeffektivnym robotam." ROBOTOTEKHNIKA 1 (2017): 55.

[15]Kuznetsov, Aleksandr Petrovich, et al. "Fenomen uravneniya van der Polya." Izvestiya vysshikh uchebnykh zavedeniy. Prikladnaya nelineynaya dinamika 22.4 (2014).

[16]Laboratory of Kinesiology and Biomechanics of the University of Tartu. Retrieved November 20, 2018 from https://www.kk.ut.ee/et/teaduskonnast

[17]Lafortune, M. A., et al. "Three-dimensional kinematics of the human knee during walking." Journal of biomechanics 25.4 (1992): 347-357.

[18]Musalimov, V. M., et al. "Modelirovaniye dinamiki oporno-dvigatel'noy sistemy." Nauchno-tekhnicheskiy vestnik informatsionnykh tekhnologiy, mekhaniki i optiki 17.6 (2017).

[19]Musalimov, V. M., L. T. Khamidullina, and P. P. Kovalenko. "Prikladnyye zadachi perechislitel'noy kombinatoriki. Uchebnoye posobiye po kursu «Diskretnaya matematika»." SPb: SPbGU ITMO (2011).

[20]Musalimov, V., et al. "Modelling of the Human Knee Joint Supported by Active Orthosis." International Journal of Applied Mechanics and Engineering 23.1 (2018): 107-120.

[21]Nguyen, Trung, Takashi Komeda, and Hung Dao. "Design and model a novel ankle foot orthosis." 3rd International Workshop on Innovative Simulation for Health Care, IWISH 2014. Dime University of Genoa, 2014.

[22]Poston, Tim, and Ian Stewart. Catastrophe theory and its applications. Courier Corporation, 2014.

[23]Rabinovich, M. I., and D. I. Trubetskov. "Vvedeniye v teoriyu kolebaniy i voln: ucheb. posobiye." (1984).

[24]Ribeiro, Ana, et al. "Modeling of the condyle elements within a biomechanical knee model." Multibody System Dynamics 28.1-2 (2012): 181-197.

[25]Stamenković, D., et al. "Methods and Principles of Determining the Footwear and Floor Tribological Characteristics." Tribology in Industry 39.3 (2017).

[26]Tondl, Aleš. Domains of attraction for non-linear systems. National Res. Inst, 1970.

[27]Tsatsos, Marios. "Theoretical and Numerical study of the Van der Pol equation." Doctoral desertation, Aristotle University of Thessaloniki 4.6 (2006).

[28]Yamaguchi, Takeshi, and Kazuo Hokkirigawa. "Experimental analysis of slip potential in Normal-style walking and Nanba-style walking." Journal of Biomechanical Science and Engineering 4.3 (2009): 468-479.

[29]Kim, C.M.; Eng, J.J. Magnitude and pattern of 3D kinematic and kinetic gait profiles in persons with stroke: Relationship to walking speed. Gait Posture 2004, 20, 140–146.

[30]Casadio, M.; Morasso, P.G.; Sanguineti, V. Direct measurement of ankle stiffness during quiet standing: Implications for control modelling and clinical application. Gait Posture 2005, 21, 410–424.

[31]Bonato, P. Wearable sensors/systems and their impact on biomedical engineering. Eng. Med. Biol. Mag. 2003, 22, 18–20

[32]Roduit, R.; Besse, P.A.; Micallef, J.P. Flexible angular sensor. IEEE Trans. Instrum. Meas. 1998, 47, 1020–1022.

7. APPENDICIES

Appendix 1. Program for finding Morse polynomials of the 4th order and calculating the coordinates of their extrema

```
function z = tip4(tips)
i=0;
tips = [ 3 1 4 2 ];
step = 0.2;
min = -2;
max = 2;
 for b = min:step:max
    for c = min:step:max
        for d = min:step:max
            for e = min:step:max
            p = [5 4*b 3*c 2*d e];
            r = roots(p);
            y = imag(r);
% The second important criterion is the inequality of the roots

                if y == 0
%inequality condition of all roots

                    t = 0;
                    for k = 1:4
                       for j = k+1:4
                           if r(k)== r(j)
                               t=1;
                           end
                       end
                    end
% Finally, if both conditions are met, the roots are sorted in ascending order
and the corresponding values are calculated along the abscissa axis. After
that, we can find out if the obtained Morse polynomials satisfies the given
transposition.

                  %sorting


                   if t == 0
                       rs = sort(r); %sorting along the x-axis
                       rs
                       q2 = rs.^5+b.*rs.^4+c.*rs.^3+d.*rs.^2+e.*rs;
                       q2
                       q2s = sort(q2); %sorting along the y-axis
                       q2s

                       u=0;
                       for j = 1:4
                          if q2(j) == q2s(tips(j));
```

```
                                u = u + 1;
                            end
                        end

                        % If the desired transposition is found, the program
proceeds to the stage of graphical output of all characteristics.

                    if u == 4;
                      format rat;
                      i=i+1;
                      p = [5 4*b 3*c 2*d e];
                      r
                      t=-2:0.01:2;
                      q = t.^5+b.*t.^4+c.*t.^3+d.*t.^2+e.*t;
                      plot(t,q);
                      hold on;
                      ymin = q2s(1);
                      ymax = q2s(4);
                      ylim([ymin ymax]);

                        % Defining of the coordinates of the extrema
along the ordinate
                    plot(rs,q2,'*');hold on;


            for k=1:length(rs)
                rs(k)=rs(k)*100;
                rs(k)=round(rs(k));
                rs(k)=rs(k)/100;

                q2(k)=q2(k)*100;
                q2(k)=round(q2(k));
                q2(k)=q2(k)/100;
            end
% display the parameters on the window with the graph
            annotation(gcf,'textbox',...
               'Position',[0 1 0 0],...
               'LineStyle', 'none',...
               'FitHeightToText','on',...
               'FontSize',16,...
               'String',{'b=','c=','d=','e=','  ','x',rs});
            annotation(gcf,'textbox',...
               'Position',[0.05 1 0 0],...
               'LineStyle', 'none',...
               'FitHeightToText','on',...
               'FontSize',16,...
               'String',{b,c,d,e,'  ','y',q2});
            title(['q = t^5 + (',num2str(b),')*t^4 +
(',num2str(c),')*t^3 + (',num2str(d),')*t^2 + (',num2str(e),')*t
'],'FontSize',16);
            xlabel (['Tipe: ',num2str(tips)],'FontSize',16);
```

```
 % maximize window

          scrsz = get(0,'ScreenSize');
          set(gcf,'Position',[1 1 scrsz(3) scrsz(4)]);
          saveas(gcf,[num2str(i),'.emf'],'emf');
          close;

                      end
                   end
                end
             end
          end
       end
 end
end
```

Appendix 2. Technical parameters of the equipment

Smart DX characteristics	DX 100
Infrared digital cameras per datastation	up to 4
Sensor Resolution	0,3 Mpixel
Acquisition frequency at maximum resolution	140fps
Maximum acquisition frequency	280fps
Accuracy/Volume	<0,2mm on 2x2x2m

Appendix 3. Anthropometric data

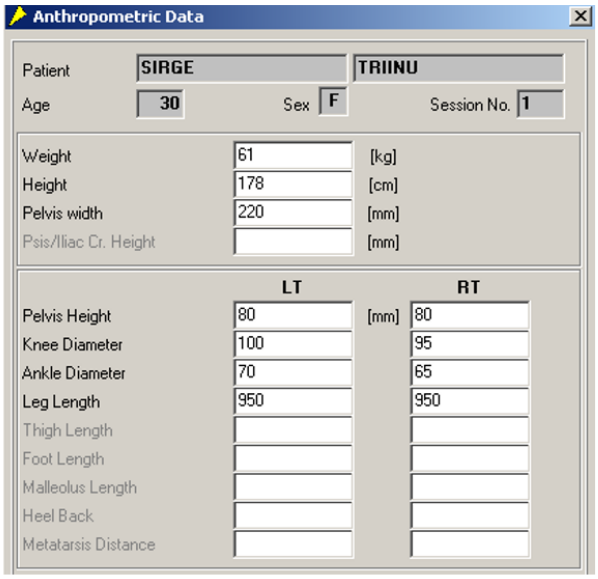

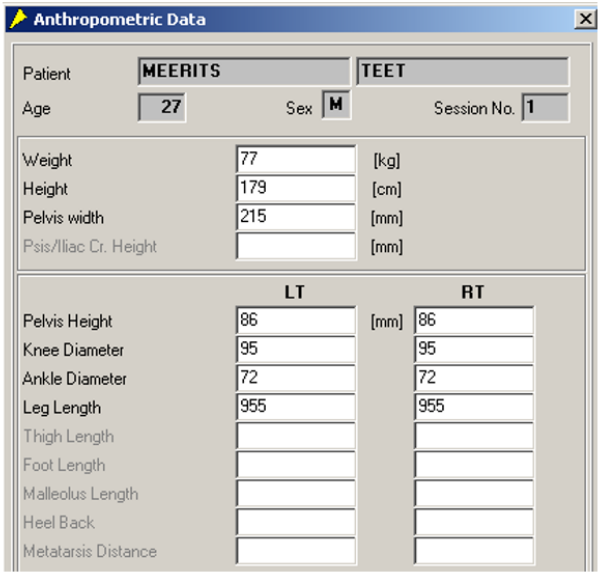

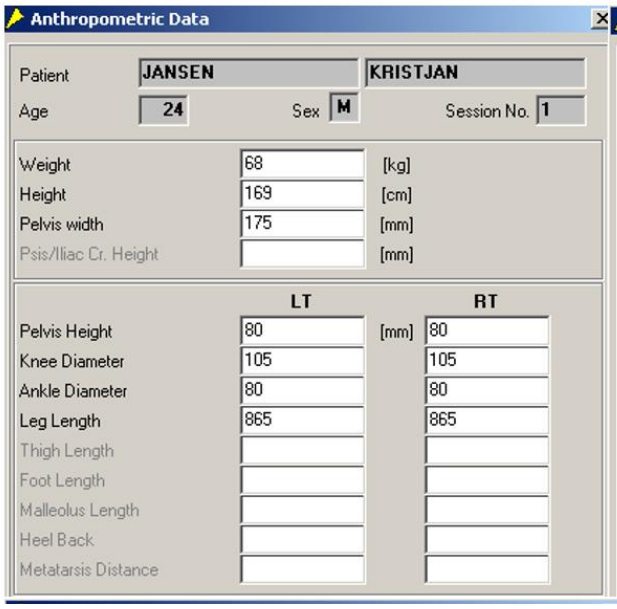

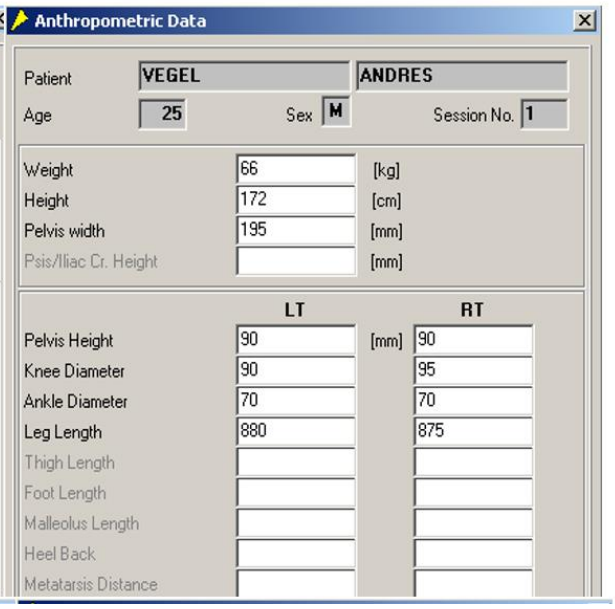

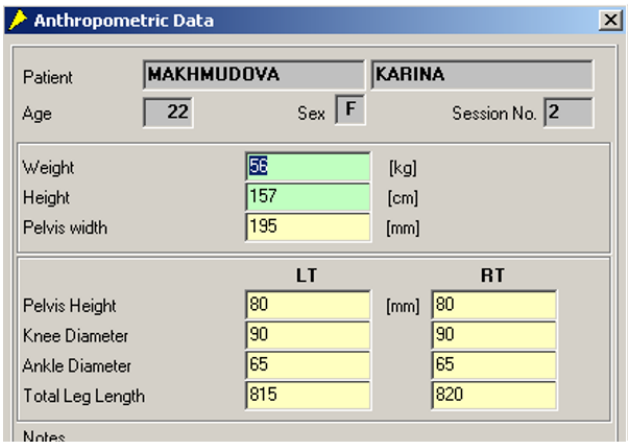
Anthropometric Data
Patient MAKHMUDOVA KARINA
Age 22 Sex F Session No. 2
Weight 56 [kg]
Height 157 [cm]
Pelvis width 195 [mm]
LT RT
Pelvis Height 80 [mm] 80
Knee Diameter 90 90
Ankle Diameter 65 65
Total Leg Length 815 820
Notes

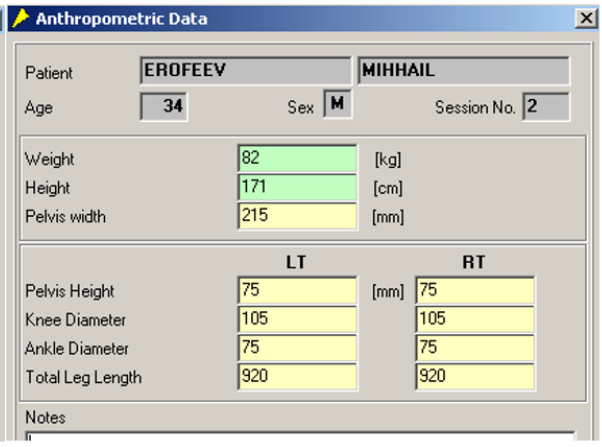
Anthropometric Data
Patient EROFEEV MIHHAIL
Age 34 Sex M Session No. 2
Weight 82 [kg]
Height 171 [cm]
Pelvis width 215 [mm]
LT RT
Pelvis Height 75 [mm] 75
Knee Diameter 105 105
Ankle Diameter 75 75
Total Leg Length 920 920
Notes

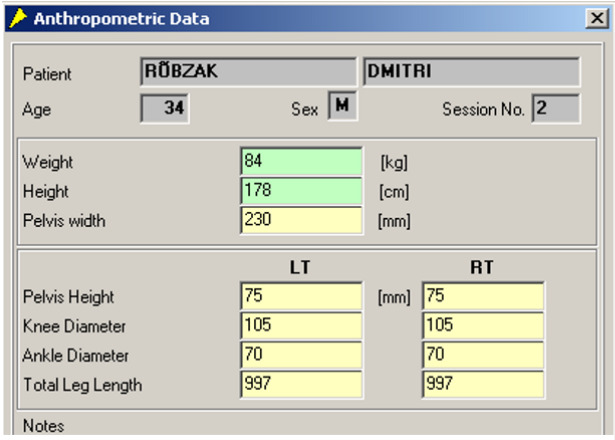
Anthropometric Data
Patient RÕBZAK DMITRI
Age 34 Sex M Session No. 2
Weight 84 [kg]
Height 178 [cm]
Pelvis width 230 [mm]
LT RT
Pelvis Height 75 [mm] 75
Knee Diameter 105 105
Ankle Diameter 70 70
Total Leg Length 997 997
Notes

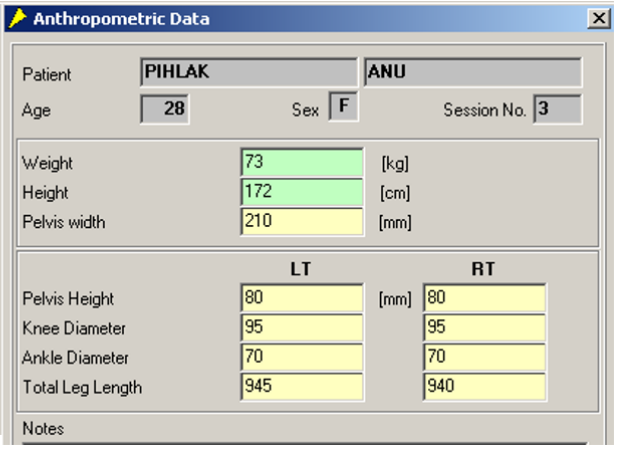
Anthropometric Data
Patient PIHLAK ANU
Age 28 Sex F Session No. 3
Weight 73 [kg]
Height 172 [cm]
Pelvis width 210 [mm]
LT RT
Pelvis Height 80 [mm] 80
Knee Diameter 95 95
Ankle Diameter 70 70
Total Leg Length 945 940
Notes

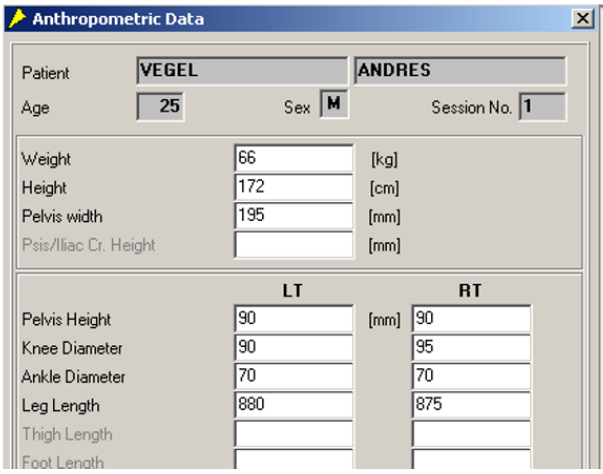
Anthropometric Data
Patient VEGEL ANDRES
Age 25 Sex M Session No. 1
Weight 66 [kg]
Height 172 [cm]
Pelvis width 195 [mm]
Psis/Iliac Cr. Height [mm]
LT RT
Pelvis Height 90 [mm] 90
Knee Diameter 90 95
Ankle Diameter 70 70
Leg Length 880 875
Thigh Length
Foot Length

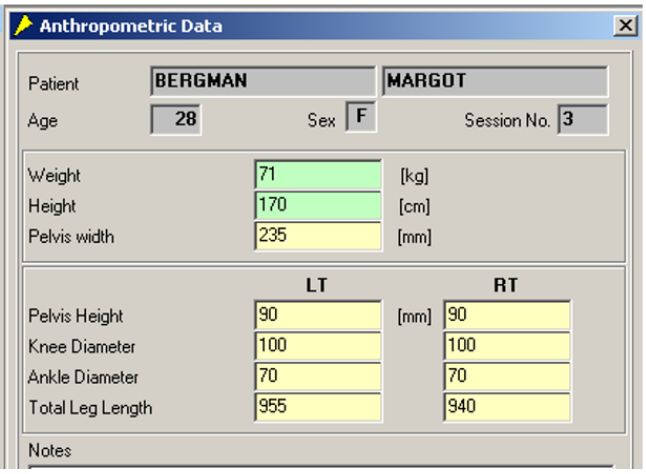
Anthropometric Data
Patient BERGMAN MARGOT
Age 28 Sex F Session No. 3
Weight 71 [kg]
Height 170 [cm]
Pelvis width 235 [mm]
LT RT
Pelvis Height 90 [mm] 90
Knee Diameter 100 100
Ankle Diameter 70 70
Total Leg Length 955 940
Notes

Appendix 4. Experimental data

LABORATORY of KINESIOLOGY and BIOMECHANICS

TARTU UNIVERSITY

CLINICAL REPORT

SURNAME:	SIITAM	**FILE NAME:**	702xxb02
NAME:	STEN	**TRIAL DATE:**	6/20/2017
AGE:	23	**TRIAL DESCRIPTION:**	Normal Walking Group 1
PATHOLOGY:	CONTROL	**PROTOCOL:**	Anatomical

TEMPORAL PARAMETERS

	RT	LT	NORMAL VALUES RT	NORMAL VALUES LT
STANCE TIME [%]	60.6	59.1	59.6 ± 1.2	59.3 ± 1.8
SWING TIME [%]	39.4	40.9	40.4 ± 1.2	40.7 ± 1.8
DOUBLE SUPP. TIME [%]	10.9	9.1	13.4 ± 1.1	8.3 ± .6
STANCE TIME [s]	0.66	0.65	0.63 ± .021	0.626 ± .042
SWING TIME [s]	0.43	0.45	0.426 ± .016	0.429 ± .023
STRIDE TIME [s]	1.09	1.1	1.056 ± .026	1.055 ± .052
CADENCE [step/min] [Hz]	109.591		113.845 ± 4.305	

DISTANCE PARAMETERS

	RT	LT	NORMAL VALUES RT	NORMAL VALUES LT
STEP LENGTH [m]	0.663	0.752	0.619 ± .004	0.74 ± .019
VELOCITY [m/s]	1.3	1.295	1.33 ± .062	1.331 ± .066
SWING VELOCITY [m/s]	3.295	3.165	3.296 ± .137	3.275 ± .184
STRIDE LENGTH [m]	1.417	1.424	1.404 ± .074	1.402 ± .06
STEP WIDTH [m]	0.13	0.139	0.11 ± .026	0.128 ± .011
MEAN VELOCITY [m/s]	1.297		1.33 ± .064	

SAGITTAL KINETICS

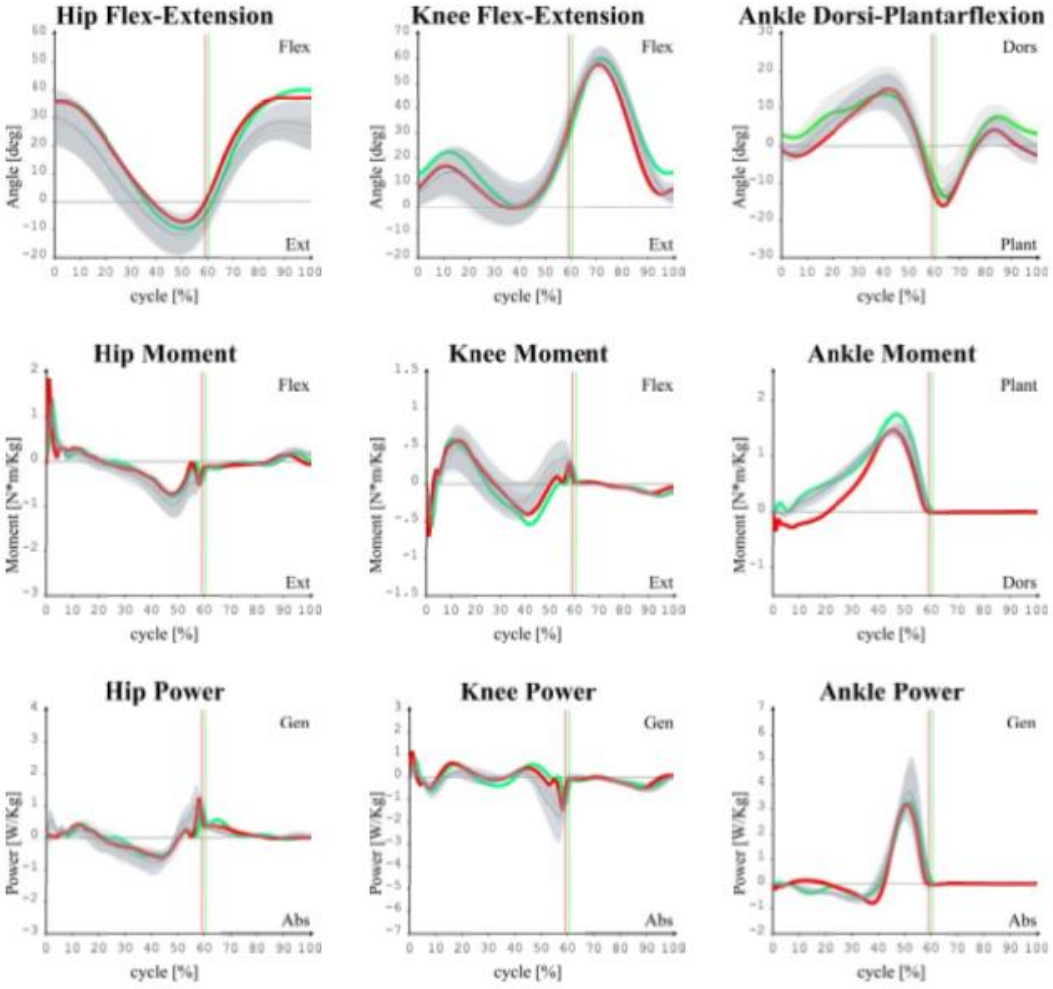

GROUND REACTION FORCE

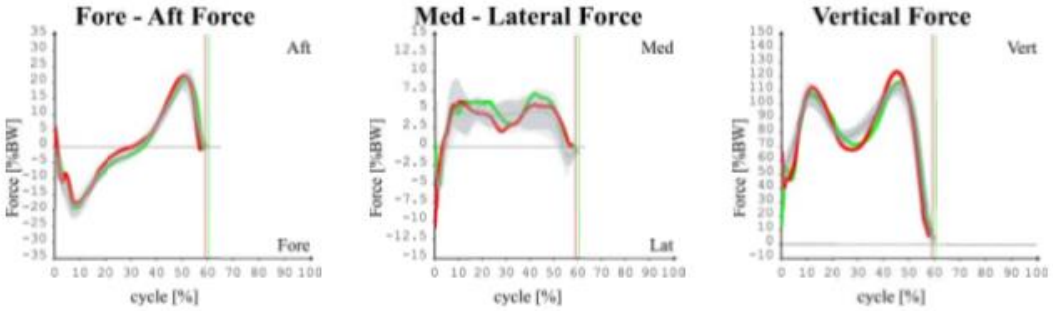

CoP

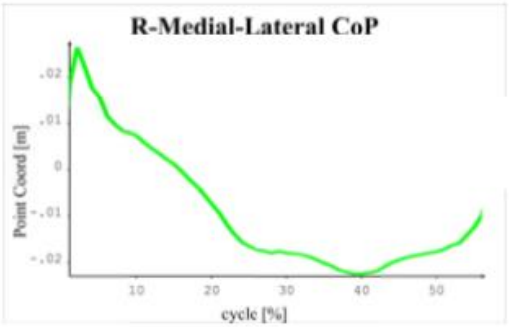

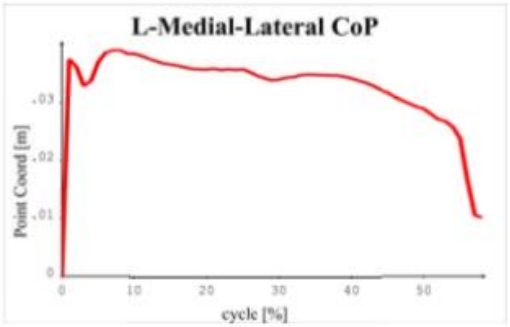

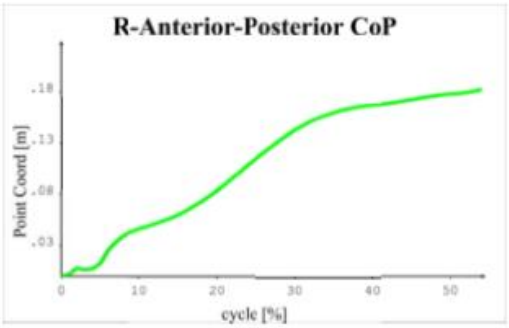

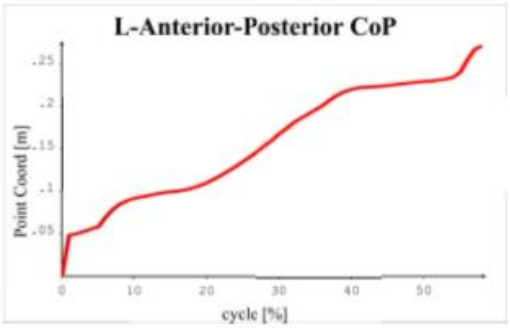

Shoulder Kinematics

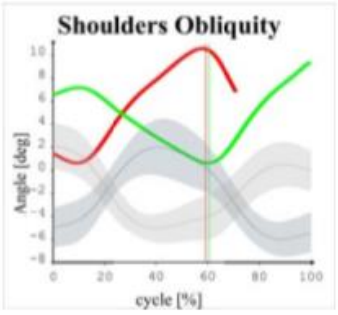

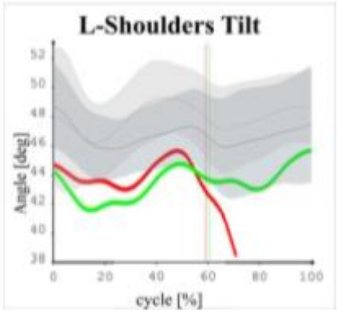

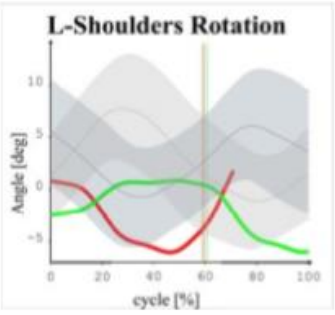

LABORATORY of KINESIOLOGY and BIOMECHANICS

TARTU UNIVERSITY

CLINICAL REPORT

SURNAME:	RAVA	**FILE NAME:**	701xxb02
NAME:	ANNI	**TRIAL DATE:**	6/20/2017
AGE:	26	**TRIAL DESCRIPTION:**	Normal Walking Group 1
PATHOLOGY:	CONTROL	**PROTOCOL:**	Anatomical

TEMPORAL PARAMETERS

	RT	LT	NORMAL VALUES RT	NORMAL VALUES LT
STANCE TIME [%]	58.7	57.7	59.6 ± 1.2	59.3 ± 1.8
SWING TIME [%]	41.3	42.3	40.4 ± 1.2	40.7 ± 1.8
DOUBLE SUPP. TIME [%]	9.3	9.3	13.4 ± 1.1	8.3 ± .6
STANCE TIME [s]	0.54	0.56	0.63 ± .021	0.626 ± .042
SWING TIME [s]	0.38	0.41	0.426 ± .016	0.429 ± .023
STRIDE TIME [s]	0.92	0.97	1.056 ± .026	1.055 ± .052
CADENCE [step/min] [Hz]	127.073		113.845 ± 4.305	

DISTANCE PARAMETERS

	RT	LT	NORMAL VALUES RT	NORMAL VALUES LT
STEP LENGTH [m]	0.65	0.685	0.619 ± .004	0.74 ± .019
VELOCITY [m/s]	1.454	1.388	1.33 ± .062	1.331 ± .066
SWING VELOCITY [m/s]	3.519	3.283	3.296 ± .137	3.275 ± .184
STRIDE LENGTH [m]	1.337	1.346	1.404 ± .074	1.402 ± .06
STEP WIDTH [m]	0.1	0.114	0.11 ± .026	0.128 ± .011
MEAN VELOCITY [m/s]	1.421		1.33 ± .064	

RT side
LT side
RT norm
LT norm

KINEMATICS

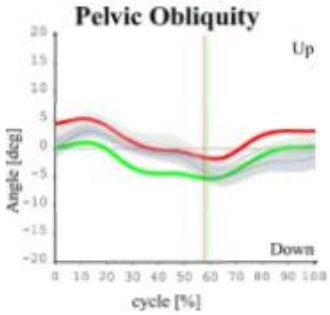

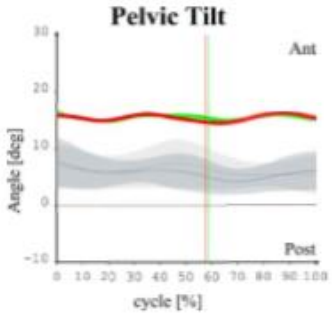

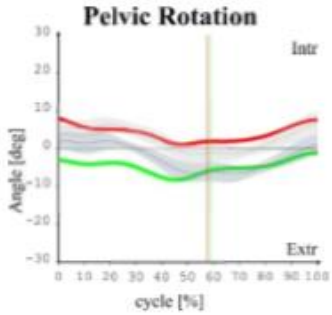

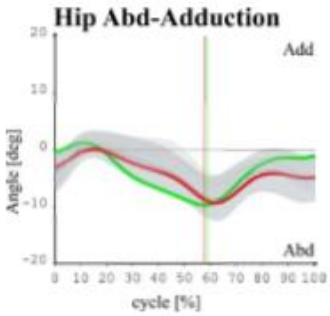

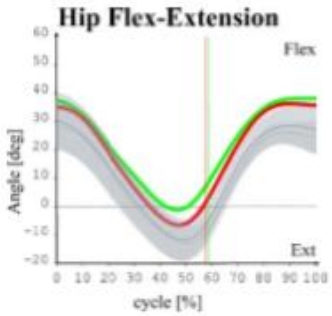

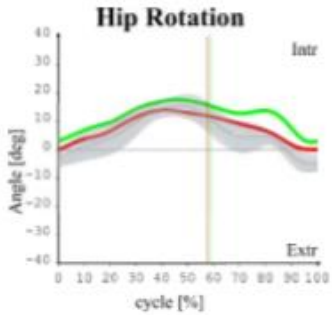

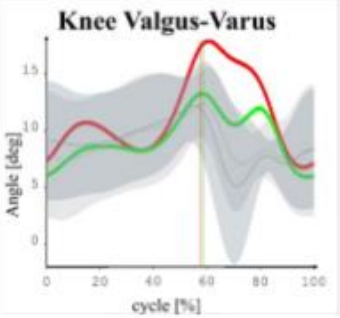

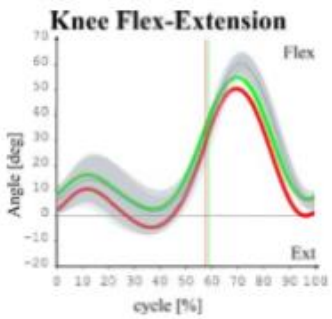

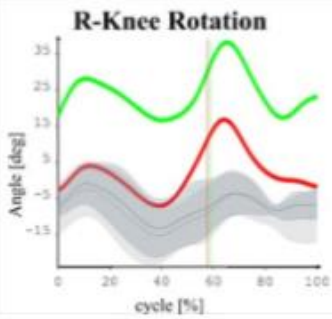

OFFSET ANGLES

Pelvic Obliquity	-2.933	
Pelvic Rotation	-4.576	
Pelvic Tilt	20.423	
Hip Abd-Add	-6.894	-3.652
Hip Intra-Extr	8.028	9.67
Hip Fless-Est	13.708	9.28
Knee Fless-Est	0.272	-7.335
Foot Progression	-16.861	-14.618
Ankle Dors-Plant	4.616	3.605

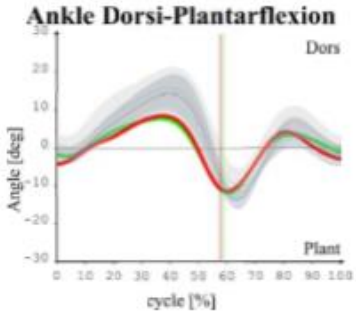

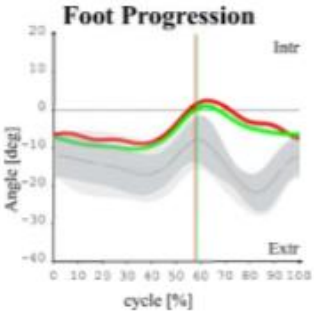

SAGITTAL KINETICS

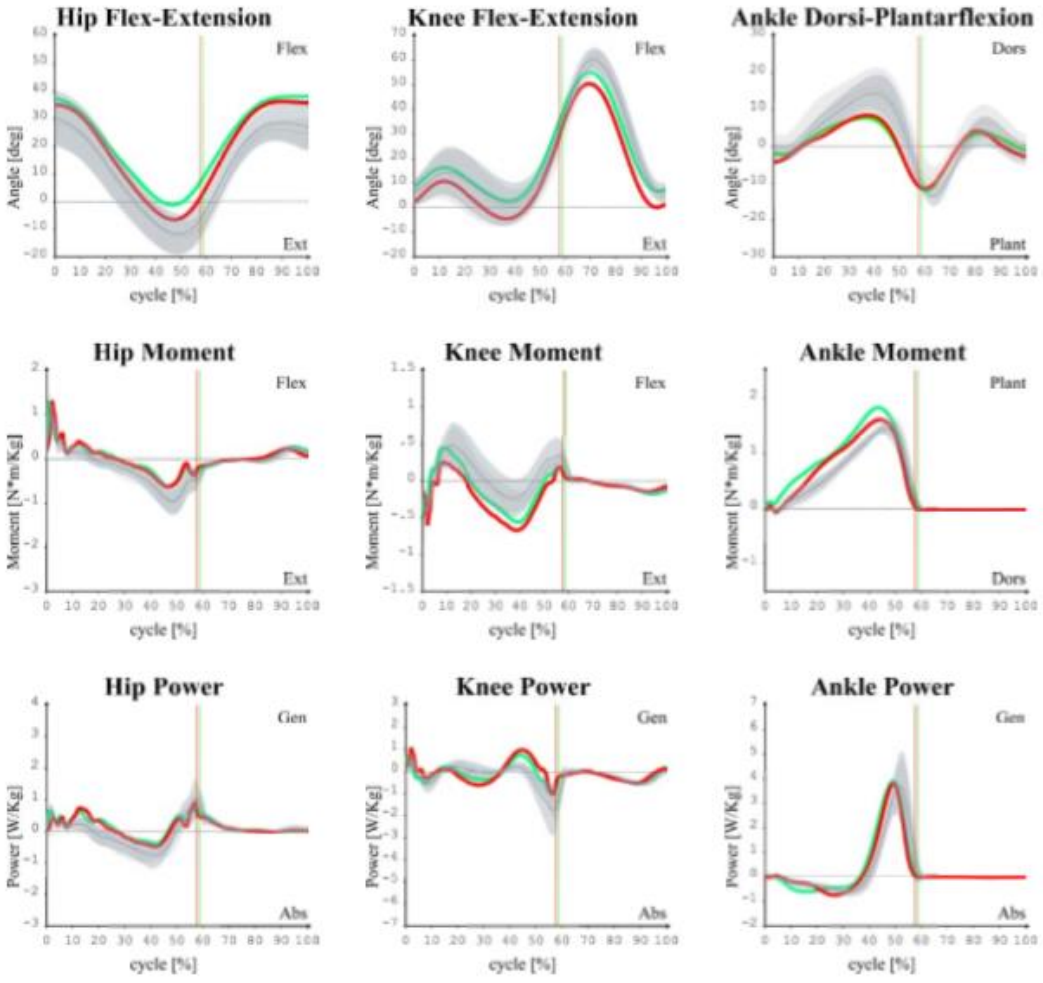

GROUND REACTION FORCE

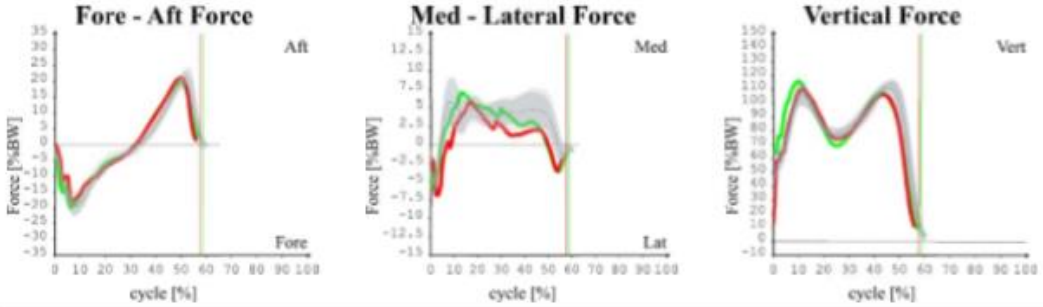

CoP

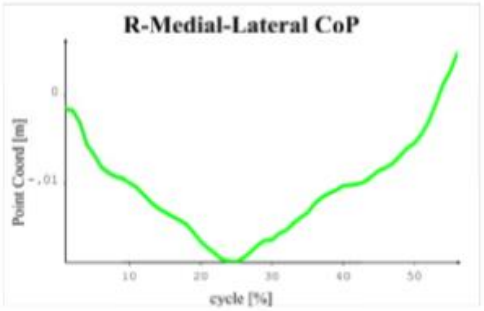

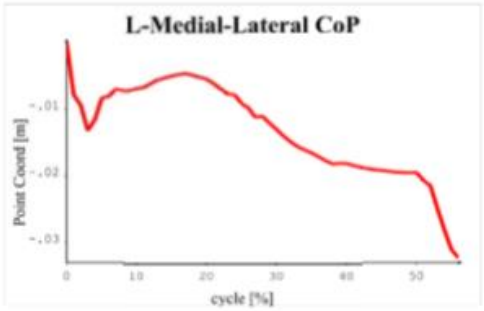

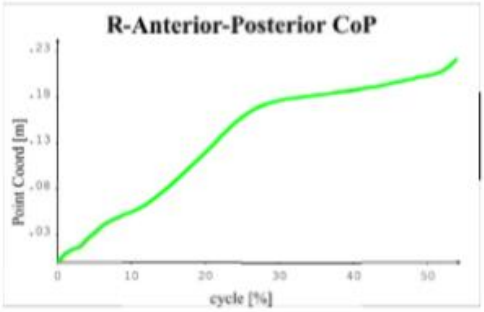

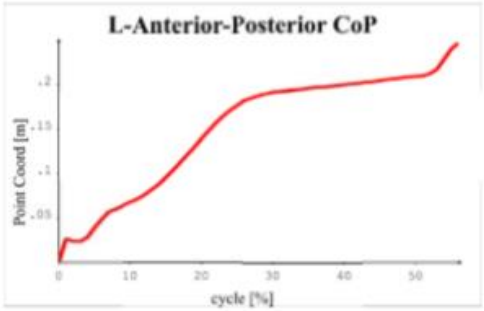

Shoulder Kinematics